Wigner crystallization in a polarizable medium

G. Rastelli and S. Ciuchi
Istituto Nazionale di Fisica della Materia and Dipartimento di Fisica Università dell'Aquila, via Vetoio, I-67010 Coppito-L'Aquila, Italy
(Received 25 June 2004; revised manuscript received 7 December 2004; published 11 May 2005)

We present a variational study of the two- and three-dimensional Wigner crystal phase of large polarons. The method generalizes that introduced by S. Fratini and P. Quémerais [Mod. Phys. Lett. B **12** 1003 (1998)]. We take into account the Wigner crystal normal modes rather than a single mean frequency in the minimization procedure of the variational free energy. We calculate the renormalized modes of the crystal as well as the charge polarization correlation function and polaron radius. The solid phase boundaries are determined via a Lindemann criterion, suitably generalized to take into account the classical-to-quantum crossover. In the weak electron-phonon coupling limit, the Wigner crystal parameters are renormalized by the electron-phonon interaction, leading to a stabilization of the solid phase for low polarizability of the medium. Conversely, at intermediate and strong coupling, the behavior of the system depends strongly on the polarizability of the medium. For weakly polarizable media, a density crossover occurs inside the solid phase when the renormalized plasma frequency approaches the phonon frequency. At low density, we have a renormalized polaron Wigner crystal, whereas at higher densities the electron-phonon interaction is weakened irrespective of the *bare* electron-phonon coupling. For strongly polarizable media, the system behaves as a Lorentz lattice of dipoles. The abrupt softening of the internal polaronic frequency predicted by Fratini and Quemerais is observed near the actual melting point only at very strong coupling, leading to a possible liquid polaronic phase for a wider range of parameters.

DOI: 10.1103/PhysRevB.71.184303 PACS number(s): 71.30.+h, 71.38.−k, 71.45.−d

I. INTRODUCTION

As it was first proposed by Wigner last century[1] the long-range Coulomb interaction is able to stabilize a crystal of electrons, which eventually melts upon increasing the density at a quantum critical point. Experiments done on heterostructures[2] and quantum Monte Carlo simulations confirm this scenario.[3,4] The presence of impurities is known to stabilize the crystal phase in two dimensions.[5] Another mechanism that could help the stabilization of the crystal phase is the effect of a polar material. As a single electron moves in a polar crystal, it polarizes its environment creating a new quasiparticle: a Fröhlich large polaron, with an enlarged effective mass.[6,7] One expects then an enlargement of the Wigner crystal phase.

Interesting properties of the liquid phase in polar doped semiconductors arise also due to the interaction with the polarization, as, for example, the mixing between plasmons and longitudinal optical (LO) phonons.[8] Such a mixing can be explained by assuming a long-range interaction between the carriers and optical lattice vibrations of the Fröhlich type.[9] The resulting coupled LO-phonon-plasmon modes (CPPMs) are found in polar semiconductors (*n*-type GaP or *p*-type GaAs).[10] Another interesting playground for this kind of physics is the surface polaron, i.e., electron close to the surface of a polar crystal, which has been intensively studied especially for intermediate electron-phonon coupling α, as in InSb where $\alpha \sim 4.5$,[11] or in AgCl where $\alpha \sim 3$.[12] It has been also observed that the gate materials (SiO_2, Al_2O_3 in organic thin films in field transistors) are polar dielectrics and the interaction between the electrons and the surface phonons of the polar dielectric is relevant.[13]

The aim of this work is to study the stabilization of the Wigner crystal phase and its properties in the presence of a polarizable medium. We consider a general model in which the key feature is the presence of long-range interactions that arise from direct Coulomb interactions between electrons and from the polarizable medium.

The presence of long-range interactions, high polarizability, and low carrier density is also a common feature of high-temperature superconductors. Of course, in these materials, short-range interactions and lattice effects play an important role. Nonetheless, polarons have been detected by optical measurements in the antiferromagnetic insulating phase of both super-conducting and parent cuprates.[14–16] Moreover, some evidence of strong electron-phonon coupling effects has been given recently in the underdoped regime.[17] An interesting physics is introduced when studying these materials by the fact that the carrier concentration can be varied from very low to sufficiently high density. Prediction on optical properties and more specifically the behavior of the so-called midinfrared band (MIR) by varying the doping has been proposed according polaronic models[18,19,31] as well as its interpretation as charge ordering in stripes.[20] A similar behavior has been also found in the optical properties of potassium doped barium bismutate.[21]

When we consider a system composed of many interacting large polarons we are faced with the problem of screening of *both* electron-electron (e-e) and electron-phonon (e-ph) interactions as we increase the carrier density. A density crossover is therefore expected when the doping concentration is varied so that the plasma frequency approaches the optical longitudinal phonon frequency ω_{LO}.

At high density, phonons cannot follow the much faster plasma oscillations of the electron gas and therefore they do not contribute to the screening of the e-e interactions. On the other hand, the electronic density fluctuations screen the e-ph interaction leading to the undressing of the electrons from

their polarization clouds. As a consequence, the polaronic mass renormalization is hugely reduced.[22] In this case, the plasma frequency of the pure electron gas $\omega_P^2=4\pi e^2\rho/m$ is renormalized by the high-frequency dielectric constant ε_∞

$$\omega_{P,H}^2=\frac{\omega_P^2}{\varepsilon_\infty}. \tag{1}$$

In the high-density region, the self energy has been studied by a perturbative approach for weak e-ph coupling ($m_{\rm pol}\simeq m$) in the metallic phase.[22] The validity of this approach is ruled by the condition of $\omega_{LO}^2\ll\omega_P^2/\varepsilon_\infty$, since in this regime $\omega_P^2/\varepsilon_\infty$ is representative of electron-density fluctuations. In this case, the electron screening weakens the *effective* e-ph coupling constant and it is argued that the perturbative approach is suitable also for semiconductors that have intermediate values of the *bare* e-ph coupling in the low doping phase. The same results have been obtained at weak and intermediate couplings by a ground-state study.[23] An approach that is able to span the strong e-ph coupling regime has been presented in Ref. 24, where an untrapping transition is found by increasing the density via the plasmon screening of the e-ph interaction. There it is concluded that there is no polaron formation at high density, irrespective of the strength of the bare e-ph coupling constant.

At low density, the phonon energy scale (phonon-frequency) exceeds the electronic energy scale (plasma frequency). In this limit, the phonons can follow the oscillations of the slower electrons and they screen the e-e interaction. Thus, the frequency of the electron collective modes is renormalized by the static dielectric constant ε_0. Moreover, in the case of intermediate and strong e-ph coupling, polarons are formed[25] so that the appropriate expression for the general renormalized plasma frequency becomes

$$\omega_{P,L}^2=\frac{m}{m_{\rm pol}}\frac{\omega_P^2}{\varepsilon_0}, \tag{2}$$

where $m_{\rm pol}$ is the polaron mass. In the case of GaAs, the mass renormalization because of the e-ph interaction is negligible, and usually Eq. (2) is used to interpret the experimental data with m, the band mass of the carriers, in place of $m_{\rm pol}$.[10]

In Ref. 26 an approximation is developed that allows one to study a system of many interacting large polarons in the intermediate- and/or low-density regime for weak and intermediate coupling strengths. The phonon degrees of freedom are eliminated by a generalized Lee-Low-Pines transformation[27] obtaining an effective pair potential between electrons, which is nonretarded, with a short-range *attractive* term and a long-range Coulomb repulsive term, statically screened by ε_0. The role of the inverse polarizability parameter $\eta=\varepsilon_\infty/\varepsilon_0$ is evident in Ref. 26. In the case of $\eta\ll 1$, which is hereafter reported as the high-polarizability regime, repulsive interaction and the retarded phonon-mediated attractive interaction are comparable, leading to a softening of the energy of the collective modes at a finite value of the wave vector k, signaling a charge-density wave instability. The attractive interaction term between the electrons plays a crucial role also at very low density where the ground state can be bipolaronic below a certain value of the polarizability parameter[35] or can undergo a solid-liquid phase transition similar to the Wigner crystallization (WC).[28] In Refs. 29 and 30, a large polaron crystal (LPC) is studied using a path-integral scheme. In Ref. 30, for $\eta=1/6$ (high-polarizability regime), the authors conclude that in the weak and intermediate e-ph coupling regimes at $T=0$ the LPC melts toward a polaron liquid, but in the strong coupling regime a phonon instability appears near the melting. The authors argue this behavior from the softening of a long wavelength collective mode due to the e-e dipolar-interaction. A study that shows the presence of a long-range order is not necessary for this kind of scenario has been presented in Ref. 31 for a simplified model of a classical liquid of interacting dipoles, which are the polarons treated *à la* Feynman. The dipolar mode (internal frequency) is renormalized by the mean field of the other dipoles, and it is shown to soften as the density increases, leading to the dissociation of the dipole (polaron).

The present work generalizes the approach of Ref. 30 using a formalism that allows one to span from a high- ($\eta\ll 1$) to low-polarizability regime ($\eta\simeq 1$). We calculate the boundaries of the solid phase in three as well as in two dimensions. We also calculate, within the solid phase, the correlation function between the electron density and the charge polarization density. Our results confirm the relevant role of the parameter η in the strong e-ph coupling regime. According to the values of this parameter, two distinct behaviors are found:

(i) the high-polarizability regime in which we found a scenario similar to that of Ref. 30, i.e., the melting of the crystal is driven by the instability of the internal polaronic mode. Interestingly our more quantitative prediction push the instability-driven melting toward very strong couplings, leaving the possibility of a liquid polaronic phase for a wider range of parameters.

(ii) the low-polarizability regime, studied here even at strong coupling, in which we found that the undressing transition argued in the liquid phase[24] occurs also in the solid phase. Nonetheless e-ph interaction is able to stabilize the crystal against the liquid phase even for moderately polarizable mediums.

This paper is organized as follows: in Sec. II we illustrate the model and the approximations used, we introduce the quantities of interest, and we also discuss the Lindemann criterion used to determine the transition temperature. In Sec. III, we present the results in the three-dimensional (3D) case. In Sec. IV, the results of the two-dimensional (2D) case are compared to the those in 3D. The conclusions are reported in Sec. V. Appendices contain technical details of the calculations.

II. MODEL AND METHOD

A. The model

The model describes a system of N interacting electrons in a D-dimensional space, which are coupled to longitudinal (undispersed) optical phonons. The Hamiltonian of the model is a generalization of that introduced by Fröhlich for a

single large polaron[32] to N-large polarons.[22] We consider electrons as distinguishable particles. This approximation is justified inside the solid phase, where the overlap between the wave functions of different localized electrons is negligible.[33] Using the path integral technique[34] phonons can be easily traced out taking advantage of their Gaussian nature, and we end up with the following partition function:[29]

$$\mathcal{Z} = \oint \prod_{\iota} \mathcal{D}[\vec{r}_{\iota}(\tau)] e^{-(1/\hbar)\mathcal{S}_{eff}}, \tag{3}$$

where $\oint$ means the functional integration over all cyclic space-time paths of the particles $\vec{r}_{\iota}(\tau)$ between zero and $\beta = \hbar/k_B T$. The effective electron action reads

$$\mathcal{S}_{eff} = \mathcal{S}_K + \mathcal{S}_{e-e} + \mathcal{S}^{\text{self}}_{e-ph-e} + \mathcal{S}^{\text{dist}}_{e-ph-e} + \mathcal{S}_J, \tag{4}$$

where

$$\mathcal{S}_K = \int_0^{\beta} d\tau \sum_{\iota} \frac{1}{2} m |\dot{\vec{r}}_{\iota}(\tau)|^2, \tag{5}$$

$$\mathcal{S}_{e-e} = \frac{e^2}{2\varepsilon_{\infty}} \int_0^{\beta} d\tau \sum_{\iota \neq j} \frac{1}{|\vec{r}_{\iota}(\tau) - \vec{r}_j(\tau)|}, \tag{6}$$

$$\mathcal{S}^{\text{self}}_{e-ph-e} = -\frac{\omega_{LO}(1-\eta)e^2}{4\varepsilon_{\infty}} \int_0^{\beta} d\tau \int_0^{\beta} d\sigma \sum_{\iota} \frac{D_o(\tau-\sigma)}{|\vec{r}_{\iota}(\tau) - \vec{r}_{\iota}(\sigma)|}, \tag{7}$$

$$\mathcal{S}^{\text{dist}}_{e-ph-e} = -\frac{\omega_{LO}(1-\eta)e^2}{4\varepsilon_{\infty}} \int_0^{\beta} d\tau \int_0^{\beta} d\sigma \sum_{\iota \neq j} \frac{D_o(\tau-\sigma)}{|\vec{r}_{\iota}(\tau) - \vec{r}_j(\sigma)|}, \tag{8}$$

$$\mathcal{S}_J = \beta \frac{(e\rho_J)^2}{2\varepsilon_0} V \int \frac{d\vec{r}}{r} - \int_0^{\beta} d\tau \sum_{\iota} \int d\vec{r} \frac{e^2 \rho_J/\varepsilon_0}{|\vec{r}_{\iota}(\tau) - \vec{r}|}. \tag{9}$$

Here e^2 is the electron charge, m is the electron band mass, and V is the volume. $(e\rho_J)$ is the static jellium charge density. The integration of phonons leads to the appearance of retarded e-e interaction terms Eqs. (7) and (8), where the phonon propagator is

$$D_o(\tau) = \frac{\cosh(\omega_{LO}[\beta/2 - \tau])}{\sinh(\beta\omega_{LO}/2)}. \tag{10}$$

Using polaronic units (p.u.) ($\hbar\omega_{LO}$ for energy, $1/\omega_{LO}$ for imaginary time τ and $\sqrt{\hbar/m\omega_{LO}}$ for lengths) $\mathcal{S}_{e-ph-e}$ becomes proportional to the dimensionless e-ph coupling constant α defined as

$$\alpha = \frac{e^2}{\sqrt{2}} \frac{1-\eta}{\varepsilon_{\infty}} \sqrt{\frac{m}{\hbar^3 \omega_{LO}}}, \tag{11}$$

whereas $\mathcal{S}_{e-e}$ will be proportional to the e-e coupling constant

$$\alpha_e = \frac{\sqrt{2}e^2}{\varepsilon_{\infty}} \sqrt{\frac{m}{\hbar^3 \omega_{LO}}}, \tag{12}$$

the ratio $\alpha_e/\alpha = 2/(1-\eta)$ is thus solely determined by $\eta = \varepsilon_{\infty}/\varepsilon_0$; when $\eta \simeq 1$ the Coulomb repulsion overwhelms the attraction mediated by phonons, while they become comparable for $\eta \ll 1$. Therefore, in the Fröhlich model, the inverse polarizability parameter rules the relative weight between the repulsive and attractive (phonon-mediated) interactions. This attraction can lead to a bipolaronic ground state as $\alpha > \alpha_c(\eta)$.[35] Roughly speaking, this condition implies strong couplings $\alpha > \alpha_c$ *and* high polarizability $\eta < \eta_c$, where $\alpha_c = 9.3$ and $\eta_c = 0.131$ in 3D, $\alpha_c = 4.5$ and $\eta_c = 0.158$ in 2D case.[35] We have investigated the system for two values of η, representative, respectively, of the high- and low-polarizability regimes and several values of the e-ph coupling α. We choose, respectively, $\eta = 1/6$ as in Ref. 30, which gives $\alpha_e/\alpha = 2.4$ and $\eta = 0.90519$ so that the coupling α_e/α is increased by a factor of ten.[36] For these values of η, no bipolaron ground state exists.

B. Harmonic variational approximation in the solid phase

We generalize the harmonic variational approach originally introduced in Ref. 29 to study the model [Eq. (4)]. First of all we recall here the variational theory in the path-integral formalism. Let us consider a suitable trial action $\mathcal{S}_T$, which depends on some variational parameters. Substituting $\mathcal{S}_{eff}$ with $\mathcal{S}_T$ in Eq. (3) we obtain the partition function $\mathcal{Z}_T$ for the trial action and the free energy associated with it $\mathcal{F}_T = -k_B T \ln \mathcal{Z}_T$. Then the exact free energy can be expressed as

$$\mathcal{F} = \mathcal{F}_T - k_B T \ln \langle e^{-(1/\hbar)\Delta\mathcal{S}} \rangle_T, \tag{13}$$

where $\Delta\mathcal{S} = \mathcal{S}_{eff} - \mathcal{S}_T$ and the mean value $\langle \ldots \rangle_T$ is

$$\langle \cdots \rangle_T = \frac{1}{\mathcal{Z}_T} \oint \prod_{\iota} \mathcal{D}[\vec{r}_{\iota}(\tau)] (\cdots) e^{-(1/\hbar)\mathcal{S}_T}. \tag{14}$$

The variational free energy is obtained by a cumulant expansion of the logarithm appearing in Eq. (13). At first order in $\Delta\mathcal{S}$ it reads

$$\mathcal{F}_V = \mathcal{F}_T + \frac{1}{\beta} \langle \Delta\mathcal{S} \rangle_T, \tag{15}$$

where $\mathcal{F}_V \geqslant \mathcal{F}$. To define a suitable trial action we proceed in two steps, as in Ref. 29. First we treat the self-interaction term $\mathcal{S}^{\text{self}}_{e-ph-e}$ of Eq. (7) *a la Feynman*.[37,38] Therefore, we substitute $\mathcal{S}^{\text{self}}_{e-ph-e}$ with $\mathcal{S}_{\text{Feyn}}$

$$\mathcal{S}_{\text{Feyn}} = \frac{(v^2 - w^2)mw}{8} \sum_{\iota} \int_0^{\beta} d\tau \int_0^{\beta} d\sigma D_V(\tau-\sigma) |\vec{r}_{\iota}(\tau) - \vec{r}_{\iota}(\sigma)|^2 \tag{16}$$

v and w are the two variational parameters. The variational propagator $D_V(\tau)$ is given by Eq. (10) with w replacing ω_{LO}. We remind that S_{Feyn} Eq. (16) can be obtained by integrating out an action where each electron interacts elastically [$K_T = m(v^2 - w^2)$] with a fictitious particle of mass $M_T = m[(v^2/w^2) - 1]$. Then v is the internal frequency and $1/\mu$

$=1/m+1/M_T$ is the reduced mass of the two-particle system.

As a second step, we treat the $\mathcal{S}_{e-e}$, $\mathcal{S}_J$ Eqs. (6) and (9) and the distinct part ($\mathcal{S}^{\text{dist}}_{e-ph-e}$) Eq. (8) of $\mathcal{S}_{eff}$ in Eq. (4) by means of a harmonic approximation. Expressing the position of the electrons around the Wigner lattice points as $\vec{r}_\iota=\vec{u}_\iota+\vec{X}_\iota$, where $\vec{X}_\iota$ are the vectors of the Bravais lattice (bcc in 3D, hexagonal in 2D) and omitting the constant terms of the solid-phase potential energy, we obtain the following harmonic variational action:

$$\mathcal{S}_T=\mathcal{S}_K+\mathcal{S}_{\text{Feyn}}+\mathcal{S}^H_J+\mathcal{S}^H_{e-e}+\mathcal{S}^{H,\text{dist}}_{e-ph-e}, \tag{17}$$

where

$$\mathcal{S}_K=\int_0^\beta d\tau\sum_\iota \frac{1}{2}m|\dot{\vec{u}}_\iota(\tau)|^2, \tag{18}$$

$$\mathcal{S}^H_{e-J}+\mathcal{S}^H_{e-e}=\int_0^\beta d\tau\sum_\iota \frac{1}{2}m\frac{\omega_W^2}{\varepsilon_0}|\vec{u}_\iota(\tau)|^2 + \int_0^\beta d\tau\frac{e^2}{2\varepsilon_\infty}\sum_{\iota\neq j}\vec{u}_j(\tau)\overline{\mathcal{I}_{ij}}\vec{u}_\iota(\tau), \tag{19}$$

$$\mathcal{S}^{H,\text{dist}}_{e-ph-e}=-\frac{\omega_{LO}e^2}{4\varepsilon}\sum_{\iota\neq j}\int_0^\beta d\tau\int_0^\beta d\sigma D_o(\tau-\sigma)\vec{u}_j(\sigma)\overline{\mathcal{I}_{ij}}\vec{u}_\iota(\tau). \tag{20}$$

In Eq. (19), the Wigner frequency is defined as usual in 3D as $\omega^2_{W,3D}=\omega_P^2/3$ [for the 2D case see Eq. (B14) in Appendix B]. The force constants $[\overline{\mathcal{I}_{ij}}]_{\alpha\beta}$ are obtained through a harmonic expansion for the Coulomb potential (see Appendix B). In our calculations, we neglect the anharmonic terms in $\Delta\mathcal{S}$ of Eq. (15), therefore we get

$$\mathcal{F}_V=\mathcal{F}_T+\frac{1}{\beta}\langle\mathcal{S}^{\text{self}}_{e-ph-e}-\mathcal{S}_{\text{Feyn}}\rangle_T. \tag{21}$$

We have minimized $\mathcal{F}_V/N$ varying w, v at given a density and temperature, keeping α and η fixed. Minimization is constrained by a convergence condition on the Gaussian integrals appearing in $\mathcal{F}_V$. The constrained minimization procedure is described in Appendix C.

So far, the discussed scheme appears very similar to the one of Ref. 29. However, we stress that the $\mathcal{F}_V$, which we have minimized to obtain the variational parameter v and w, contains the heterointeraction terms $\mathcal{S}^H_{e-e}$ and $\mathcal{S}^{H,\text{dist}}_{e-ph-e}$, which are not included in the minimization procedure of Ref. 29. Moreover, we have also used the *whole* trial action $\mathcal{S}_T$ Eq. (17) to calculate the mean electronic fluctuation, which we have used in the Lindemann rule, as explained in Sec. II C.

C. Lindemann rule and phase diagrams

To determine the solid-liquid transition we use the phenomenological Lindemann criterion, suitably generalized to take into account the classical-to-quantum crossover[39]

$$\frac{\langle|\vec{u}|^2\rangle_{eff}}{d^2_{\text{NN}}}=\gamma^2(\eta_q). \tag{22}$$

In the left-hand side (lhs) of Eq. (22) we have the Lindemann ratio between the mean fluctuation of the electrons around its equilibrium position and the nearest-neighbor distance d_{NN}. When it exceeds a critical value [right-hand side (rhs) of Eq. (22)], the solid melts. In Eq. (22) $\langle\ldots\rangle_{eff}$ is the average taken over $\mathcal{S}_{eff}$ Eq. (4). The average is carried out at the zeroth order in the cumulant expansion as an average over $\mathcal{S}_T$ Eq. (17).

Contrary to the classical liquid-solid transition, where the Lindemann rule predicts the full melting line using a constant $\gamma=\gamma_{cl}$, in the case of a quantum crystal an interpolating formula for γ is necessary to determine the melting line as obtained by comparing the free energies of the two phases calculated using quantum simulations.[3] Hence the analytic expansion of the quantum corrections to the classical free energy respect to the quantum parameter η_q and the zero-temperature melting density provides the interpolating function [rhs of Eq. (22)] for $\gamma(\eta_q)$.[39] η_q is defined for the pure electron gas as the ratio between zero point and thermal activation energies as

$$\eta_q=\frac{\hbar\omega_p}{2k_BT}. \tag{23}$$

We have chosen for the function $\gamma(\eta_q)$ the form of Refs. 40,41

$$\gamma(T,r_s)=\gamma_q-\frac{\gamma_q-\gamma_{cl}}{1+A\eta_q^2}. \tag{24}$$

Formula (24) has a single interpolation parameter A, which we take as $A=1.62\times10^{-2}$ in 3D[40] and $A=3\times10^{-2}$ in 2D.[41]

The chosen value of $\gamma_{cl}=0.155$ is such that the classical transition lines ($T=2/\Gamma_c r_s$ a.u.) are recovered in both the 3D ($\Gamma_c=172$ from Ref. 40) and 2D ($\Gamma_c=135$ from Ref. 41) cases. The value $\gamma_q=0.28$ is chosen to reproduce the zero temperature quantum transition in 3D ($r_s=100$ a.u. from Ref. 40) and 2D ($r_s=37$ a.u. from Ref. 41).

Roughly speaking, the transition curve is limited by the classical line $T=(2/\Gamma_c)1/r_s$ and the quantum melting $1/r_s=1/r^c$. The actual transition curve is a smooth interpolation between these two limiting behaviors. Of course, the precise knowledge of the interpolation formula (i.e., the knowledge of parameters appearing in it) is critical only for the determination of the transition line at high temperatures (see Fig. 1).

We note that the particular values of the parameters entering in Eq. (24) depend on the kind of statistics (boson, fermion) and on the system parameters only via the ratio η_q.[42] This parameter depends on the mass of the particles via ω_p, which measures the zero point energy of the oscillator, which eventually melts.[43] Therefore, to generalize the Lindemann criterion to the interacting large polaron system we are left with the alternative of choosing between the electron and the polaron effective mass in Eqs. (23) and (24).

The polaron exists as a well-defined quasiparticle when

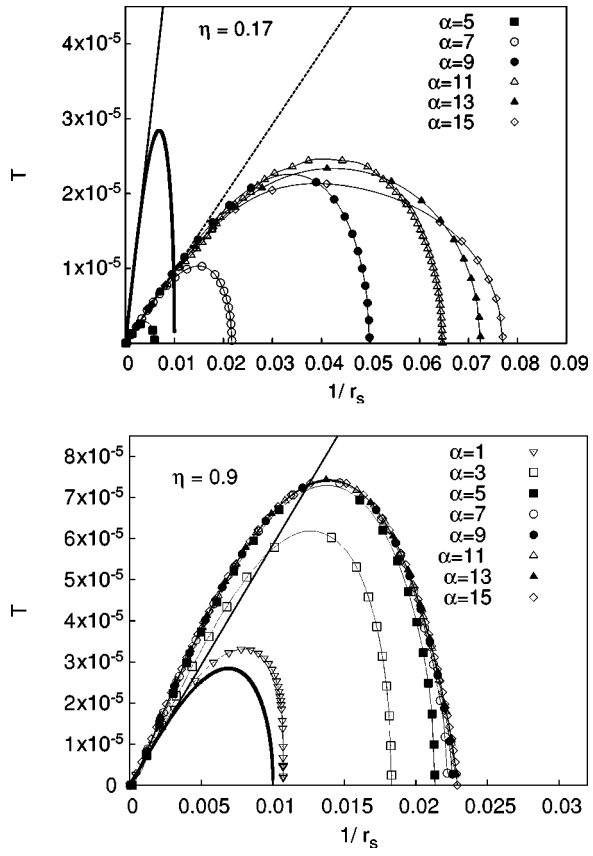

FIG. 1. Phase diagrams for a 3D LPC for $\eta=0.17$ (upper panel) and $\eta=0.9$ (lower panel). Atomic units (a.u.) are used for temperature and r_s (see text). Solid phase is enclosed below transition lines. In both the upper and lower panels, the continuous bold curve is the pure WC transition line and solid line gives the classical melting. In the upper panel, the dashed line is the renormalized classical melting.

both $k_BT \ll \hbar\omega_{LO}$[44] and $\hbar\overline{\omega}_P \ll \hbar\omega_{LO}$. The second condition relies on the effectiveness of the e-ph interaction, as explained in the introduction. Therefore, if both conditions are fulfilled, we have to replace ω_P in Eq. (23) by $\overline{\omega}_P$ given by Eq. (2). In this case, between the classical ($\eta_q \simeq 0$) and quantum melting ($\eta_q \to \infty$), we have a polaronic Wigner crystal. This is the case of the high polarizability ($\eta=0.17$).

For low polarizability ($\eta=0.9$), a crossover occurs inside the solid phase when $\hbar\overline{\omega}_P \sim \hbar\omega_{LO}$ and the coupling is intermediate or strong, as it will be discussed, in detail, later on. In this case, we still have a classical melting of polaronic quasiparticles, but the quantum melting involves the undressed electrons. In the classical regime (low density), the transition line does not depend appreciably on the quantum parameter, as γ attains its classical limit ($\eta_q \to 0$). In the quantum regime at high density and low temperatures ($\eta_q \to \infty$) the function γ Eq. (24) saturates to its quantum value γ_q and the density r_c of the quantum melting does not depend of the choice for the quantum parameter η_q. Instead, a pronounced dependency on the actual value of the quantum parameter is expected in the calculation of the melting line at high temperatures and intermediate densities.

For $\eta=0.9$ we choose the high-density estimate $\omega_P/\sqrt{\varepsilon_\infty}$ as the plasma frequency entering in Eq. (23). This choice produces, in the intermediate temperature and/or density region, an upward deviation (Fig. 1, lower panel) from the classical slope. This is a drawback of our approximation, which is, however, correct at low temperatures for both low and high density.

We finally discuss to which extent we use the Lindemann criterion in 2D and, more generally, on the applicability of the harmonic theory in 2D. This is related to the well-known problem of the existence of two-dimensional crystalline long-range order at finite temperature.[45] In a pure electron gas, for $T=0$, this problem does not arise and the properties of the system in the harmonic approximation have been studied extensively.[46,47] The general statement for the classical impossibility of 2D crystalline long-range order was first pointed out by Peierls.[48] Landau[49] gave a general argument according to which fluctuations destroy crystalline order, possessing only a one- or two-dimensional periodicity. The first microscopic treatment of the problem (not valid in case of Coulomb interaction) is due to Mermin:[45] his proof is based on Bogolyubov's inequality, which leads to the conclusions that the Fourier component of the mean density is zero for every vector k in the thermodynamic limit. Motivated by the interest of the 2D electron gas, Mermin's proof was critically re-examined for the long-range potential.[50,51] We discuss here the argument of Peierls for the 2D electron crystal. The mean-square thermal fluctuations of a generic classical particle diverges in two dimensions for an infinite harmonic crystal. At low density, we have $\eta_q \simeq 0$ and the mean electronic fluctuation can be approximated by the classical value

$$\langle u^2 \rangle_{Cl,WC} = \frac{Dk_BT}{2m\omega_P^2}\mathcal{M}_{-2}, \tag{25}$$

$$\mathcal{M}_{-2} = \int d\omega \rho\,(\omega)\frac{\omega_P^2}{\omega^2}, \tag{26}$$

where $\mathcal{M}_{-2}$ is the dimensionless second inverse moment of the density of the states (DOS) of charge fluctuation normal modes in the pure WC [$\rho(\omega)$]. Since long-wavelength acoustical vibrational modes scale as $\omega=c_sk$, the DOS is given at low energies by $\rho(\omega) \sim \omega$ for $\omega \to 0$[52] and the integral Eq. (25) diverges logarithmically. However, a lower cutoff in the frequency spectrum, which exists for a large but finite system studied in the laboratory[52] or in a computer simulation,[4,53] removes the logarithmic divergence. We have chosen a cutoff frequency that corresponds to a fixed number of particles $N \simeq 5 \times 10^5$. The dependence of the cutoff is discussed in Appendix A. There and later on it is shown that our results are cutoff independent for low temperatures and density near the quantum critical point. Therefore we will discuss 2D case only in this region.

D. Correlation functions and polaron radius

We now introduce the correlation functions between the electron and the polarization densities for a system with N electrons and a measure of the polaron radius.

The polarization density vector of the medium is associated to the optical-phonon modes $Q_{\tilde{q}}$ through the relation[7]

$$\vec{P}(\vec{r}) = \sum_{\vec{k}} i \frac{\omega_{LO}}{\sqrt{4\pi\bar{\varepsilon}V}} \frac{\vec{k}}{|k|} e^{i\vec{k}\vec{r}} Q_{\vec{k}}. \tag{27}$$

The induced charge density is defined by[7]

$$n_i(\vec{r}) = -\frac{1}{e}\vec{\nabla} \cdot \vec{P}(\vec{r}). \tag{28}$$

Correlation between a given electron and the induced charge density can be defined as

$$C_1(\vec{r}', \vec{r}) = \frac{\langle \rho_1(\vec{r}) n_i(\vec{r}') \rangle}{\langle \rho_1(\vec{r}') \rangle} \tag{29}$$

with $\rho_1(\vec{r}) = \delta(\vec{r} - \vec{r}_1)$. In Eq. (29) we have chosen the appropriate normalization for the correlation function between *one* electron and the polarization. Integrating out the phonons we arrive at the following expression in which we express all quantities in terms of averages weighted by the effective action [Eqs. (4)]

$$C_1(\vec{r}', \vec{r}) = \frac{1}{\bar{\varepsilon}} \int_0^\beta d\tau \frac{\omega_{LO}}{2} D_o(\tau) \frac{\langle \rho_1(\vec{r}) \rho(\vec{r}', \tau) \rangle_{eff}}{\langle \rho_1(\vec{r}) \rangle_{eff}}. \tag{30}$$

In Eq (30) $\rho(\vec{r}', \tau)$ is the path density defined by

$$\rho(\vec{r}', \tau) = \delta[\vec{r}' - \vec{r}_1(\tau)] + \sum_{i \neq 1} \delta[\vec{r}' - \vec{r}_i(\tau)], \tag{31}$$

where we have explicitly separated the contribution $\rho_1(\vec{r}', \tau)$ due to the electron 1 from the remainder. The first contribution in rhs of Eq. (31) gives rise to a self term in the correlation function Eq. (30) given by

$$C_1^{\text{self}} = \frac{1}{\bar{\varepsilon}} \int_0^\beta d\tau \frac{\omega_{LO}}{2} D_o(\tau) \frac{\langle \rho_1(\vec{r}) \rho_1(\vec{r}', \tau) \rangle_{eff}}{\langle \rho_1(\vec{r}) \rangle_{eff}}. \tag{32}$$

Note that in the limit of a single isolated polaron, this correlation function reduces to the one evaluated in Ref. 44. Assuming an electron at origin ($\vec{r}=0$), we have C_1^{self} depending only on $\vec{r}'$. The radial-induced charge density $g(r)$ can be defined as

$$g(r) = r^{D-1} \int d^D\Omega \, C_1^{\text{self}}(\vec{r}). \tag{33}$$

Using this function, we can define, as a measure of the polaronic radius, the square root of the second moment of $g(r)$

$$R_p = \left[\int_0^\infty dr \, r^2 g(r) \right]^{1/2}. \tag{34}$$

The actual calculation for the mean values appearing in Eq. (32) are carried out at the zeroth order of the variational cumulant expansion. Explicit calculations are reported in Appendix E.

III. RESULTS IN 3D

Here we compare the low ($\eta=0.9$) and high ($\eta=1/6$) polarizability cases in 3D. For each polarizability, the electron-phonon coupling constant α spans from weak to strong coupling regime: $\alpha=1$, 3, 5, 7, 9, 11, 13, 15. Phase diagrams obtained through the Lindemann criterion are shown in Fig. 1 where the solid-liquid transition lines of the LPC are compared to that of the pure Wigner crystal. Density is expressed in terms of the adimensional parameter $r_s^3 = a_o^3/[(4\pi/3)\rho]$, where a_o is the Bohr radius with ($m = m_e, \varepsilon_\infty = 1$). A common feature of both the low- and high-polarizability cases is the enlargement *in density scale* of the solid phase as far as e-ph coupling increases. However, in both cases, the solid phase cannot be stabilized for any density by increasing the e-ph interaction, and the quantum melting point saturates at a maximum value when the e-ph coupling is very strong. To illustrate this different behavior it is worth introducing a simplified model.

A. Simplified model

In the simplified model, introduced in Ref. 30, the electrons interact with each other and with *all* the fictitious particles ($\{\vec{R}_i\}$) with mass M_T, which represent the polarization of the medium. After integration of the fictitious particles, we obtain the effective electronic Lagrangian $\mathcal{L}_{eq}$. The effective harmonic Lagrangian $\mathcal{L}_{eq}$ generated by the simplified model corresponds exactly to the Lagrangian of the action $\mathcal{S}_T$ Eq. (17) with the parameter $w = \omega_{LO}$. This approximation restricts the space of variational parameters and therefore gives rise to a worse estimate for the free energy. Nonetheless, it allows one to describe the physics of the system in a simplified fashion.

Each WC branch is splitted in two branches for the LPC and the frequencies of the system are given by the two roots $\Omega_\pm^2(\omega_{s,\vec{k}})$ (Eqs. (24) and (25) of the work[30]), where $\omega_{s,\vec{k}}$ are the WC frequencies with wave vector $\vec{k}$ and branch index s. The expression for the mean fluctuation $\langle u^2 \rangle_{eq}$ of electrons around their equilibrium value in the simplified model is easily obtained by inserting $w = \omega_{LO}$ in the variational expression $\langle u^2 \rangle_T$ [see Appendix D, Eqs. (D2)–(D4)]. The $\Omega_\pm$ branches give rise to a natural splitting of contributions to the fluctuation

$$\frac{\langle u^2 \rangle_{eq}}{d_{\text{NN}}^2} = \frac{\langle u^2 \rangle_+}{d_{\text{NN}}^2} + \frac{\langle u^2 \rangle_-}{d_{\text{NN}}^2}. \tag{35}$$

In the low-density regime of the simplified model,[30] i.e., when phonons are much faster than density fluctuations, the spectrum can be decomposed into the renormalized WC frequencies $\tilde{\Omega}_-(\omega_{s,\vec{k}})$ and the polaronic optical frequencies $\tilde{\Omega}_+(\omega_{s,\vec{k}})$, which can be obtained by expanding the general solutions $\Omega_\pm^2(\omega_{s,\vec{k}})$ with respect to the parameter $\epsilon_{s,\vec{k}}$ defined as

$$\epsilon_{s,\vec{k}} = \omega_{s,\vec{k}}^2/(\varepsilon_0 v^2), \tag{36}$$

which is small for *all* frequencies $\omega_{k,s}$ of WC normal modes at the low-density regime.

The first part of the spectrum represents the *low* frequencies associated with the oscillation of the center of mass ($m_{\text{pol}} = m + M_T$) of the two-particle system, i.e., the electron

and its relative fictitious particle (polarization), whereas the second part of the spectrum describes the dipolar modes associated with the internal motion of the oscillating electron-fictitious particle system (Fig. 1 of Ref. 30). Dipolar modes are weakly dispersed around the frequency $\omega_{\rm pol}$ [Eq. 25 of Ref. 30] defined as the $k=0$ mode of the polaronic branches. This represents the internal frequency of oscillation of the electron inside its polarization well.

B. Classical and renormalized quantum melting

Now let us consider the classical transition. This transition is located in the low-density regime of the simplified model. Using the low-density expansion for the spectrum $[\tilde{\Omega}_-(\omega_{s,\vec{k}}), \tilde{\Omega}_+(\omega_{s,\vec{k}})]$, it is possible to associate each term, $\langle u^2\rangle_+$ and $\langle u^2\rangle_-$, to a definite degree of freedom of the two-particle system, i.e., to the fluctuation of the center of mass

$$\langle u^2\rangle_- \simeq \int d\omega\rho(\omega)\,\frac{\hbar D\coth\left[\hbar\left(\sqrt{\frac{m}{\varepsilon_0 m_{\rm pol}}}\right)\omega/2k_BT\right]}{2m_{\rm pol}\left(\sqrt{\frac{m}{\varepsilon_0 m_{\rm pol}}}\right)\omega} \tag{37}$$

and to the fluctuation associated with the internal dipolar mode with $\vec{\rho}=\vec{u}-\vec{R}_T$ and reduced mass μ

$$\langle u^2\rangle_+ \simeq \left(\frac{M_T}{m+M_T}\right)^2\frac{\hbar D}{2\mu\omega_{\rm pol}}\coth\left(\frac{\hbar\omega_{\rm pol}}{2k_BT}\right). \tag{38}$$

In this case we can easily estimate the ratio between electronic fluctuations in LPC and WC by taking into account only the renormalized WC spectrum, i.e., the fluctuation associated with the center of mass Eq. (37). Using Eq. (25) we have $\langle u^2\rangle_{\rm LPC}/\langle u^2\rangle_{\rm WC}=1/\epsilon_0$ then by Lindemann criterion Eq. (22) and by Eq. (25) at a given density, the critical temperature ratio also equals $1/\epsilon_0$

$$\frac{T^{Cl}_{\rm LPC}}{T^{Cl}_{\rm WC}}=\frac{1}{\varepsilon_0}. \tag{39}$$

Therefore, the slope of the classical transition line is lowered by the same factor, as can be seen in Fig. 1 (upper panel), where ε_0 is appreciably large.

The quantum melting is ruled by the zero point fluctuations of the electronic oscillations. A zero temperature estimate for the pure WC gives

$$\langle u^2\rangle_{\rm WC}=\frac{\hbar D}{2m\omega_P}\mathcal{M}_{-1}, \tag{40}$$

$$\mathcal{M}_{-1}=\int d\omega\rho(\omega)\frac{\omega_P}{\omega}, \tag{41}$$

where $\mathcal{M}_{-1}$ is the dimensionless inverse moment of the WC DOS. If we consider only the renormalized WC spectrum Eq. (37), and we take into account Eq. (40), we get for the LPC

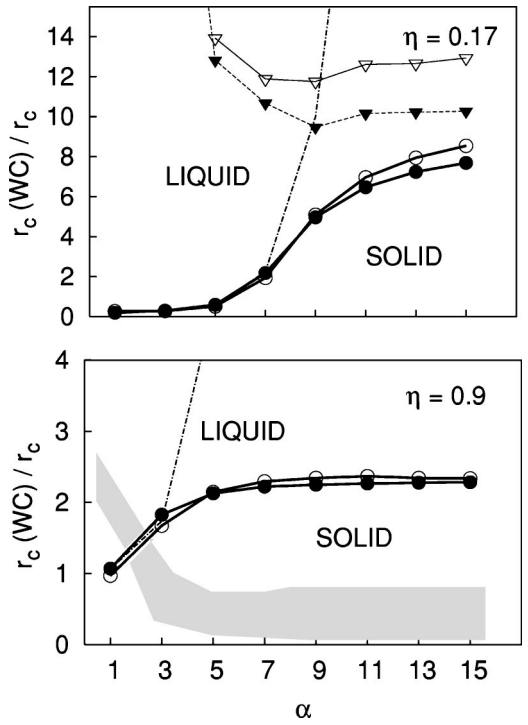

FIG. 2. Zero-temperature phase diagram in the 2D (open symbols) and 3D (solid symbols) cases. In 2D α has been scaled according the zero density limit. Circles are the scaled quantum melting r_c vs e-ph coupling constant α. The dashed line is the renormalized quantum melting transition curve from Eq. (43). Upper panel: $\eta=0.17$. Triangles locate the softening of $\omega_{\rm pol}$. Lower panel: $\eta=0.9$. The shaded area encloses the crossover region inside the solid phase.

$$\frac{\langle u^2\rangle_{Q,\rm LPC}}{\langle u^2\rangle_{Q,\rm WC}}=\left(\frac{m\varepsilon_0}{m_{\rm pol}}\right)^{1/2}\left[\frac{r_s}{r_s({\rm WC})}\right]^{3/2}, \tag{42}$$

then using Lindemann criterion we obtain at the quantum critical point (r_s-r_c)

$$\frac{r_c({\rm WC})}{r_c}=\frac{m_{\rm pol}}{m\varepsilon_0}. \tag{43}$$

Eq. (43) generalizes the result of the Ref. 29 where the Lindemann rule was discussed within a mean-field approach.

At high polarizability $\langle u^2\rangle_-$, Eq. (37) is the leading term in the mean electronic fluctuation $\langle u^2\rangle_{eq}$ Eq. (35) near the quantum melting for small and intermediate couplings $\alpha\leqslant 7$. In this case, the quantum melting density scales as Eq. (43). Note that at weak coupling the mass renormalization is weak, but phonon screening through ε_0 dominates, leading to quantum melting at lower densities than in a purely electronic Wigner crystal (upper panel of Figs. 1 and 2). At low polarizability Eq. (43) is valid up to $\alpha\simeq 3$ (Fig. 2).

On increasing the coupling, $m_{\rm pol}$ scales as $\sim\alpha^4$ in strong coupling and Eq. (43) predicts a divergence of the quantum melting density. As shown in Figs. 1 and 2, the quantum melting density saturates to an α-independent value at strong coupling, and the prediction of Eq. (43) is no longer valid.

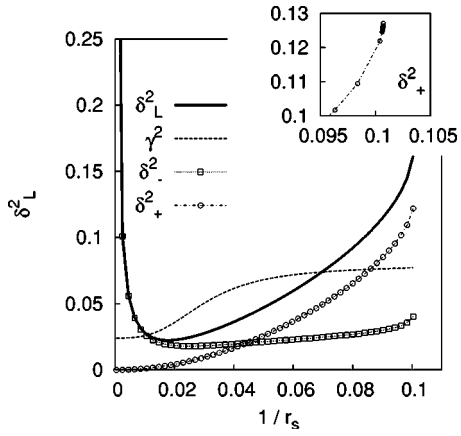

FIG. 3. The Lindemann ratio (solid line) and the function γ (dashed line) for $\eta=0.17$ and $\alpha=13$, $T=1.10^{-5}$(a.u.). Contributions $\delta^2_{\pm}=\langle u^2\rangle_{\pm}/d^2_{n.n.}$ of the simplified model Eq. (35) are also shown. The inset shows the abrupt slope increase of the term δ^2_+.

We will see in Sec. III C that deviations from the prediction of Eq. (43) arise from different reasons in low- and high-polarizability cases.

C. High polarizability: Softening of internal mode

This is the case in which the polarization gives a large contribution to the total interaction energy of the system. The system can be thought of as being composed by interacting dipoles that are made by electrons surrounded by their polarization.

In the case of strong e-ph coupling we observe a saturation of the critical quantum melting density. In Fig. 3 the electronic fluctuation is reported for $\alpha=13$. Contrary to the small-intermediate coupling case, $\langle u^2\rangle_+$ Eq. (38) is now the leading term near the quantum melting. The melting density given by Eq. (43) is not a good estimate because of the contribution of polaronic optical modes, which is now important at the quantum melting. The same scenario of Ref. 30 is recovered: the optical polaronic frequencies drive the melting at strong coupling and high polarizability. Moreover we note that $\langle u^2\rangle_+ \sim (1/\omega_{\rm pol})$ and, as density approaches a critical value $\omega_{\rm pol}$ softens, inducing an abrupt increase of electron fluctuation that is dominated by the term $\langle u^2\rangle_+$ (see Fig. 3). The same behavior for $\omega_{\rm pol}$ is reported in Ref. 30 and explained in terms of the attractive interaction between the polarons (polarization catastrophe). We stress, however, that employing a more quantitative Lindemann criterion together with a self-consistent variational calculation of all Feynmans' parameters we get quantum melting in a region in which $\omega_{\rm pol}$ do not actually soften. As a result the softening of internal polaronic frequency approaches quantum melting only asymptotically for very large α (Fig. 2).

Saturation occurs to value of r_c, which seems to lie in the high-density regime where our approach could be questionable. We must stress, however, that in the pure electron gas, the parameter r_s is a measure of *both* coupling and density. Indeed r_s can be obtained from the ratio of the Fermi energy to the mean Coulomb interaction, even if scaled with the band mass and the dielectric constant of the host medium, which are anyway fixed, i.e., not density dependent. If we introduce another coupling into the system, as the e-ph interaction, the two concepts are distinct. Global interaction is not only a function of the density but is also a function of the e-ph coupling α. Now in the high-polarizability case, polarons are well defined as quasiparticles and we can use $m_{\rm pol}(\alpha)$ as effective mass while the repulsive interactions are screened by ε_0 in the low-density regime. Only in this case we can introduce a measure of the *coupling* through the parameter $r_s^*=(m_{\rm pol}/\varepsilon_0 m)r_s$. For the low-polarizability case the last assumption is not valid as explained onward. The values of r_s^* at the quantum melting (r_c^*) are reported in Table I. When the coupling $\alpha<7$ the quantum melting can be estimated thru Eq. (43), which means $r_c^*\simeq r_c(\mathrm{WC})=100$; that is, the *coupling* parameter r_c^* tends to the value of the Wigner crystal melting of a 3D electron gas. On the contrary, in the strong e-ph coupling the values of the effective coupling parameter r_c^* are much bigger than those of the density r_c due to the huge enhancement of polaron mass.

TABLE I. The critical value at the melting of the density (r_c) and coupling (r_c^*) parameters as function of α for high polarizability $\eta=0.16$.

α	r_c	r_c^*
1	510	99.8
3	334	99.3
5	168	99.5
7	46	99.8
9	20	197.5
11	15	452.2

Of course the exchange effects *at* the crystal melting are relevant and can be taken into account only phenomenologically in our harmonic approximation (see Ref. 42 and discussion in Sec. II C). However in the solid phase we must note that these effects are ruled in LPC by the parameter r_s^* rather than r_s making them much more negligible than those at the same density in the pure electron gas. To realize this fact we assume that the localized electronic wave function is a Gaussian of variance σ, then the overlap between two of these functions at distance r_s is proportional to $\exp(-r_s^2/4\sigma^2)$. Now σ in the harmonic approximation can be extimated as $\sigma^2=1/2m_{\rm pol}\omega_W$, where $\omega_W^2=\omega_{P,L}^2/3$ is the LPC Wigner frequency and $\omega_{P,L}^2$ is given by Eq. (2). Then it is then obvious that $r_s^2/4\sigma^2=\sqrt{r_s^*}/2$, a result that can be compared to the same for electron gas[33] in which appears r_s and a different coefficient because of a more elaborate variational procedure. Taking into account the data in Table I, we see that the exchange effects are, *a fortiori*, negligible in a first approximation in the case of the strong e-ph coupling, where the quantum melting occurs at a huge coupling parameter r_c^*.

In Fig. 4 we show the behavior of the polaron radius as a function of density. Although in the solid phase it remains almost constant, when approaching the melting density it suddenly increases. This behavior can be understood by taking into account that the polaron radius is essentially deter-

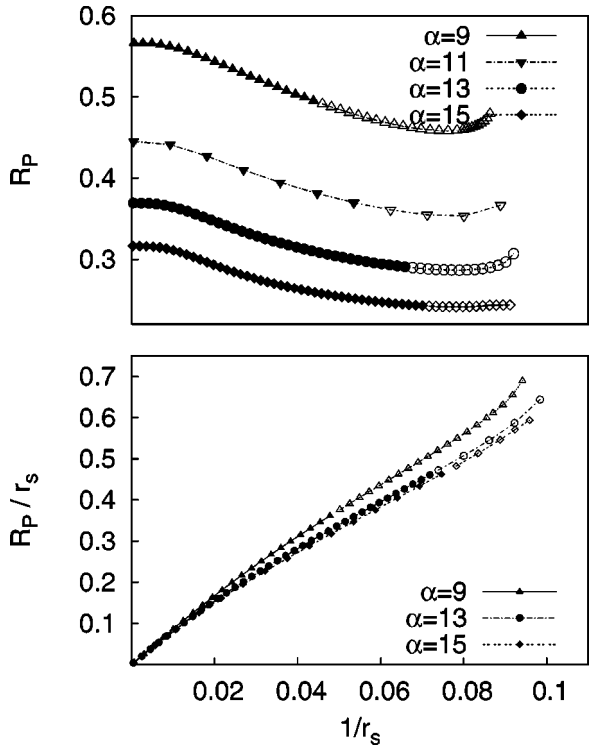

FIG. 4. Polaron radius in polaronic units (upper panel) and polaron radius scaled with r_s (lower panel) vs $(1/r_s)$ (a.u.) for different α and $\eta=0.17$ at low temperature ($T=5\times10^{-3}$ p.u.). Filled points refer to the solid phase.

mined by the diffusion in imaginary time of the electron path defined in Eq. (C16) [see also Eqs. (E4) and (E7)]. Its maximum value occurs at $\tau=\beta/2$, which diverges at the softening of the polaronic frequency ($\omega_{\rm pol}\sim0$). Polaronic clouds tend to overlap (Fig. 4, lower panel). However, the polaronic nature of each particle of the LPC is preserved up to quantum melting.

D. Low polarizability: Crossover in solid phase

In this regime ($\eta\sim1$), the repulsive interactions among electrons overwhelm the attractive interactions due to the polarizability of the background, as can be seen by the relative weight of e-e and e-ph interaction coupling constant Eqs. (11) and (12). However, self-trapping effects are still present at least at strong coupling and at low density, where electrons are localized.

Equation (43) quantitatively describes quantum melting in the low-polarizability case only at weak coupling ($\alpha\leqslant3$). When α exceeds this value, a crossover between a polaronic and nonpolaronic phase is found inside the solid phase and the estimate of Eq. (43) no longer describes quantum melting.

The low-density regime, introduced in Sec. III C, is found only for the classical part of the crystal phase, where the polarization follows adiabatically the electron and the solid phase is a Wigner crystal made of polarons with an effective mass determined by the e-ph interaction, in the way discussed for high polarizability.

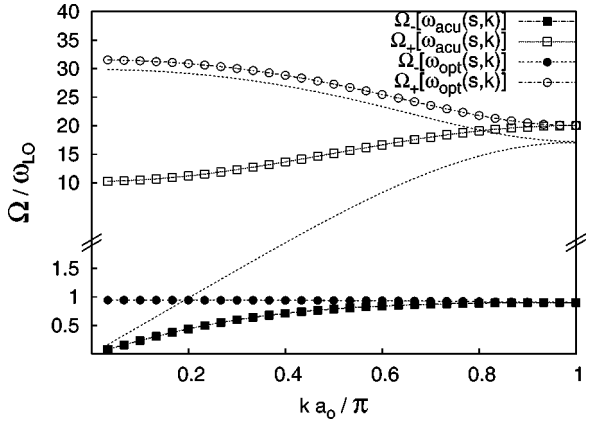

FIG. 5. Frequencies of the system in the simplified model as a function of $\vec{k}$ along the direction (100), for $\alpha=5$ and $\eta=0.9$, at $1/r_s=2\times10^{-2}$ and at $T=1.8\times10^{-5}$(a.u.). Density is close to the quantum melting. $(\Omega_-[\omega_{acu}],\Omega_+[\omega_{acu}])$ result from the splitting of $\omega_{acu}(s,k)$ the acoustical WC branch. $(\Omega_-[\omega_{opt}],\Omega_+[\omega_{opt}])$ result from the splitting of the high-frequency WC optical branch [Eqs. (44) and (45)]. For comparison the pure WC frequencies (dotted lines) are shown.

As far as the density increases (inside the solid phase), we observe that the two-energy scale, ω_{LO} of phonons and $\omega_{P,L}$ and Eq. (2) of the renormalized WC frequencies, come close and we found a crossover region *inside the solid phase*, where the electrons and polarization modes are mixed as in the liquid phase CPPM (Fig. 1 of Ref. 9 and Fig. 1 of Ref. 10). An example of the general situation is given in Fig. 5.

To estimate the density dependence of the LPC frequencies $\Omega_\pm(\omega_{s,k})$, let us substitute $\omega_{s,\vec{k}}$ with the plasma frequency ω_P. Results are reported in Fig. 6, which illustrates the density crossover. In the low-density limit $(r_s\to\infty)\Omega_-=\omega_{P,L}$ [Eq. (2)], while Ω_+ converges to $\omega_{\rm pol}\simeq v$, the internal frequency for an single polaron. In this case, the electrons are far apart, and the "external" harmonic field generated by the surrounding electrons of the crystalline array is weak ($K_e\sim e^2/r_s^3$).

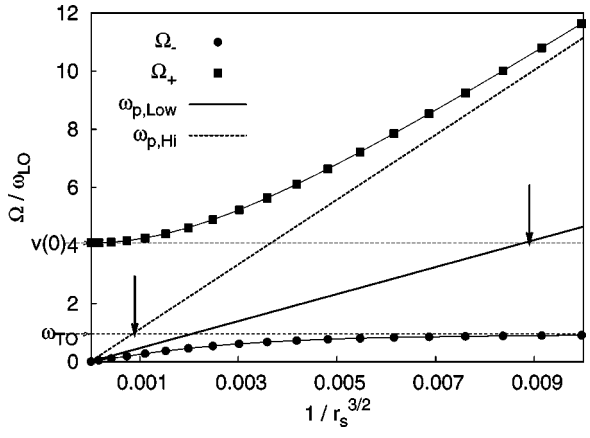

FIG. 6. Filled points are the typical frequencies of the simplified model obtained with $\omega_{s,k}=\omega_P$ for $\alpha=5$ and $\eta=0.9$. The solid line is the low-density renormalized plasma frequency [Eq. (2)]. Dashed line the high density renormalized plasma frequency Eq. (1). Arrows mark the crossover region (see text).

Therefore the frequency of electron oscillation ($\omega_P^2 \sim K_e/m$) can be lower than that of the phonon (ω_{LO}), and the polarization follows the electron oscillation. The polaron vibrates as a whole with a lower frequency $K_e/m_{\mathrm{pol}} \sim \omega_P^2(m/m_{\mathrm{pol}}\varepsilon_0)$. The polarization charge distribution is undisturbed as a first approximation, so that the value of the internal polaronic frequency ($\sim v$) of an electron inside its polarization well does not change.

By increasing the density, we approach the opposite limit of a strong external field. Now the frequency associated to this field is too large and the polarization cannot follow the electron oscillation, so that each electron becomes undressed from its polarization cloud. In this case Ω_+ approaches $\omega_P/\sqrt{\varepsilon_\infty}$, the high-density renormalized plasma frequency [Eq. (1)], while $\Omega_- \simeq \sqrt{\varepsilon_\infty/\varepsilon_0}\omega_{LO} = \omega_{TO}$ is the characteristic renormalized frequency of the polarization. We note that at low density Ω_- gives a measure of the frequency of carrier density fluctuations, whereas in the opposite limit of high density, the same role is played by Ω_+.

As we can see from Fig. 6, the crossover amplitude is determined by the conditions $\omega_{P,H} \simeq \omega_{TO}$ and $\omega_{P,L} \simeq v$. It is interesting to compare our Fig. 6 to Fig. 1 of Ref. 9. We note that the asymptotic boundary given there by the phonon frequency ω_{LO} here it is played by the internal frequency.

The renormalization crossover of the plasma frequency from the low- to high-density regime does not imply the melting of the crystal. Indeed, it is observed within the boundary of the solid phase estimated by Lindemann criterion. This behavior is even more clear once we consider the fluctuations of the position of the electrons that enter in the Lindemann criterion.

The leading term for the Lindemann ratio at the classical melting is $\delta_-^2 = \langle |u|^2 \rangle_- / d_{\mathrm{NN}}^2$, which is associated with the fluctuation of the center of mass [Eq. (37)]. Of course, in the classical region quantum fluctuations are ineffective; the electrons and its polarization cloud behave as a single classical particle with mass m_{pol}. The term $\delta_+^2 = \langle |u|^2 \rangle_+ / d_{\mathrm{NN}}^2$ associated with the internal polaronic frequencies [Eq. (38)] is indeed negligible.

To analyze the high-density region where we eventually meet the Lindemann criterion for quantum melting, we note that the condition $\epsilon_{s,\vec{k}} \gg 1$, where $\epsilon_{s,\vec{k}}$ is defined in Eq. (36), can be fulfilled by the majority of normal modes at high density. Of course, long wavelength acoustical and even "optical" modes in 2D have vanishing energies, but their spectral weight is low enough to be neglected in the following considerations. Expanding $\Omega_\pm(\omega_{s,k})$ in $1/\epsilon_{s,\vec{k}}$ we get

$$\Omega_- \simeq \sqrt{\frac{\varepsilon_\infty}{\varepsilon_0}}\omega_{LO}, \tag{44}$$

$$\Omega_+ \simeq \frac{\omega_{s,\vec{k}}}{\sqrt{\varepsilon_\infty}}. \tag{45}$$

In Fig. 5 the general solutions $\Omega_\pm(\omega_{s,k})$ are shown for all branches of the simplified model near the quantum melting.

The branches $(\Omega_-[\omega_{opt}], \Omega_+[\omega_{opt}])$ that result as splitting of optical model of the Wigner crystal $\omega_{opt}(s,k)$ are well described by an approximation of Eqs. (44) and (45).

The frequency dispersions $(\Omega_-[\omega_{acu}], \Omega_+[\omega_{acu}])$ of the modes, which originate from the splitting of acoustical branches of the Wigner crystal, are also reported. Although at short wavelength, the dispersion approaches the estimates given in Eqs. (44) and (45) the long wavelength part of the spectrum is conversely described by the low-density expansion $\tilde{\Omega}_\pm$.

Thus we have that at the quantum melting the low-energy part of the spectrum still behaves as in the low-density regime. The modes depicted in the lower part of Fig. 5 belongs to this part of the spectrum.

A measure of the wave vector below which we have this behavior can be obtained by the condition $\epsilon_{s,\vec{k}} = 1$. The associated energy scale is given by $\omega_c^2 = m\omega_{LO}^2/(\varepsilon_0 m_{\mathrm{pol}})$. Contrary to the low-density regime [Eqs. (37) and (38)], it is not possible to associate each term of the fluctuation Eqs. (D3) and (D4) with a definite degree of freedom. However, expanding the electron fluctuation with respect to the parameter $\epsilon_{s,\vec{k}}$ for the frequencies $\omega_{s,k} < \omega_c$ and with respect to the parameter $1/\epsilon_{s,\vec{k}}$ for the frequencies $\omega_{s,k} > \omega_c$ and using Eq. (35), the electron position fluctuations can be approximated by

$$\langle u^2 \rangle_- \simeq \int_0^{\omega_c} d\omega \rho(\omega) \frac{\hbar D \coth\left[\hbar\left(\sqrt{\frac{m}{m_{\mathrm{pol}}\varepsilon_0}}\right)\omega/2k_BT\right]}{2m_{\mathrm{pol}}\left(\sqrt{\frac{m}{m_{\mathrm{pol}}\varepsilon_0}}\right)\omega}, \tag{46}$$

$$\langle u^2 \rangle_+ \simeq \left(\frac{M_T}{m+M_T}\right)^2 \frac{\hbar D}{2\mu\omega_{\mathrm{pol}}} \coth\left(\frac{\hbar\omega_{\mathrm{pol}}}{2k_BT}\right) \int_0^{\omega_c} d\omega \rho(\omega) + \int_{\omega_c}^{\infty} d\omega \rho(\omega) \frac{\hbar D}{2m\frac{\omega}{\sqrt{\varepsilon_\infty}}} \coth\left(\hbar\frac{\omega}{\sqrt{\varepsilon_\infty}}/2k_BT\right). \tag{47}$$

Note that the interpretation of the fluctuations associated with electronic motion in this case is different from that valid at low density. In particular the high energy contribution [the second term of Eq. (47)] represents a Wigner crystal-like fluctuation with a low-energy cutoff. This is the largest contribution to the fluctuation at quantum melting and does not depend on e-ph interaction.

Indeed the leading term of fluctuations at quantum melting is $\langle u^2 \rangle_+$. This is due to the vanishing of the spectral weight associated with the low frequencies $\omega < \omega_c$ at high density [Eq. (46)].

The saturation of the quantum melting point can be seen in the phase diagram of Fig. 1 (lower panel). Two comments are needed. First, in the case of very low e-ph coupling, the density crossover does not occur inside the solid phase. Therefore, these arguments do not apply. The quantum melting point depends on the e-ph coupling as we have discussed in the previous section. However a saturation of the quantum melting density is observed clearly in Fig. 1 for intermediate and strong coupling. As a second point we have to emphasize

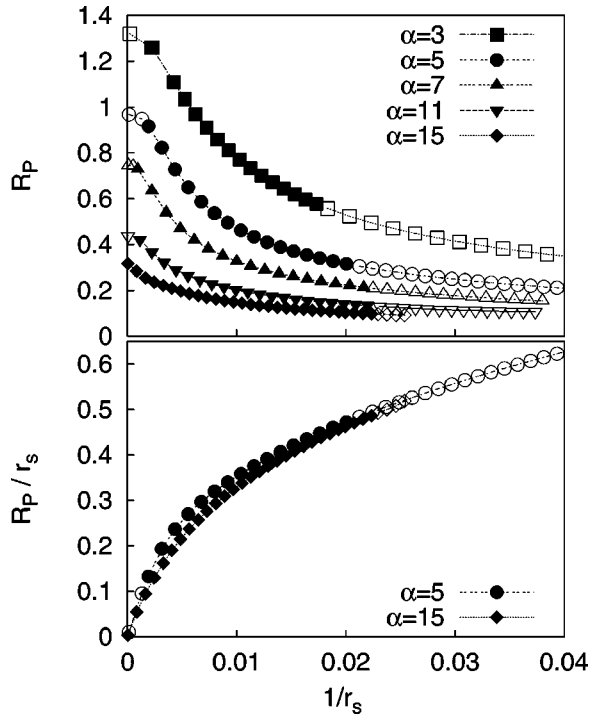

FIG. 7. Polaron radius in polaronic units (upper panel) and polaron radius scaled with r_s (lower panel) vs $(1/r_s)$ (a.u.) for different α in the case $\eta=0.9$ at low temperature ($T=5\times10^{-2}$ p.u.). Filled points refers to the solid phase.

that the quantum melting density *is not* that of a purely electronic Wigner crystal.

This fact can be explained by writing the total electron fluctuation as the sum of the two terms $\langle u^2\rangle_{\mathrm{Hi}}$ and $\langle u^2\rangle_{\mathrm{Low}}$ where $\langle u^2\rangle_{\mathrm{Hi}}$ is the contribution to fluctuations of modes having energies higher (lower) than ω_c. We note from Eq. (47) that in both LPC and WC cases $\langle u^2\rangle_{\mathrm{Hi}}$ are the same. But although in the WC case the two terms are of the same order $\langle u^2\rangle_{\mathrm{Low}}\simeq\langle u^2\rangle_{\mathrm{Hi}}$ in the LPC case $\langle u^2\rangle_{\mathrm{Low}}\ll\langle u^2\rangle_{\mathrm{Hi}}$ as far as the density increases. This is due to the renormalization of the low-energy frequencies. Therefore, the electronic fluctuation in the LPC increases more slowly with density than those of the WC. At a given density, the electronic fluctuation of the WC is greater than those of the LPC and this explains the shifting of the quantum melting toward higher densities.

The crossover is also evident in the polaron radius. In the upper panel of Fig. 7 we plot the polaron radius as defined by the Eq. (34). We see that for any value of the e-ph coupling, the polaron radius tends to decrease as far as the density is increased. We recall that as far as the renormalized plasma frequency [Eq. (2)] exceeds the phonon frequency, we enter in a region in which the polarization is adiabatically slow compared to the electronic motion. Therefore, the electronic charge appears as a static distribution whose radius decreases on increasing the density and the polaron radius follows this trend. The crossover is evident by scaling the polaron radius with r_s, as reported in the lower panel of Fig. 7 at intermediate and strong α. Note that as in the high-polarizability case at the transition $R_p/r_s\simeq0.475$.

It is possible to estimate the high-density limit of the radial distribution of the induced charge. Using the condition $\omega_o\ll\omega/\sqrt{\varepsilon_\infty}$ we have the following expression valid at low temperature ($k_BT\ll\hbar\omega_o$) (for details, see Appendix E)

$$\tilde{g}(r)\simeq\frac{1}{\varepsilon}\left[\frac{r}{\frac{\hbar}{m\omega_{LO}}}\left(1-\mathrm{erf}\sqrt{\frac{r^2}{\langle u^2\rangle}}\right)+\frac{2r^2}{\langle u^2\rangle}\frac{e^{-\frac{r^2}{2\langle u^2\rangle}}}{(2\pi\langle u^2\rangle)^{3/2}}\right]. \tag{48}$$

The first term of Eq. (48) takes into account quantum charge fluctuations that are relevant at small distances, whereas the remaining term is a classical contribution coming from the static charge distribution. Note that only the first term depends on the e-ph interaction. Therefore, the polaron radius tends to the same high-density asymptotic value for different values of the e-ph coupling α (see upper panel of Fig. 7).

As a last point we note that the crossover condition, roughly estimated as $\omega_P\sim\omega_{LO}\sim(1-\eta)^2/\alpha^2\sim0.01/\alpha^2$, shifts toward higher densities as the e-ph coupling constant α is reduced. In the weak coupling regime it lies in the liquid phase where RPA approaches in both the 3D case[22,54] and 2D case[55] can be applied. It is also worth remarking that for high polarizability and for all coupling, the polaronic crossover is located in the liquid phase according to the highest value of $\omega_{LO}\sim0.7/\alpha^2$.

IV. 2D CASE

The results obtained in the 2D case are qualitatively similar to the 3D case. Both the crossover phenomenon in the low-polarizability case and the softening of the polaronic frequency in the high-polarizability case are observed. Results are reported in the zero-temperature phase diagram of Fig. 2. In this figure, we compare the phase diagrams in 2D and 3D by scaling appropriately the 2D e-ph coupling constant following the single polaron results of Ref. 56: $\alpha_{3D}=(3\pi/4)\alpha_{2D}$. 2D and 3D melting curves scale well according to the zero-density scaling for all studied cases. A discrepancy is found in the the high-polarizability strong e-ph coupling softening of ω_{pol}. Let us first discuss the scaling at finite density.

In our variational scheme, the DOS of the WC is the peculiar difference between the 2D and 3D cases. To see this explicitly let us compare the e-ph interaction terms $\mathcal{S}^{\mathrm{self}}_{e-ph-e}$. Assuming polaronic units we get:

$$\frac{1}{\beta}\frac{\langle\mathcal{S}^{\mathrm{self}}_{e-ph-e}\rangle_{T,3D}}{3N}=-(\alpha)\frac{\sqrt{2}}{6}\int_0^{\beta/2}d\tau\frac{D_o(\tau)}{\sqrt{(\pi/2)d_{3D}(\tau)}}, \tag{49}$$

$$\frac{1}{\beta}\frac{\langle\mathcal{S}^{\mathrm{self}}_{e-ph-e}\rangle_{T,2D}}{2N}=-\left(\frac{3\pi}{4}\alpha\right)\frac{\sqrt{2}}{6}\int_0^{\beta/2}d\tau\frac{D_o(\tau)}{\sqrt{(\pi/2)d_{2D}(\tau)}}, \tag{50}$$

where the imaginary time diffusion $d(\tau)$ [Eq. (C16)] is itself a functional of the DOS. We note from Eqs. (49) and (50) that the free-energy functional scales explicitly as in the single polaron case[56] by scaling the coupling constant α.

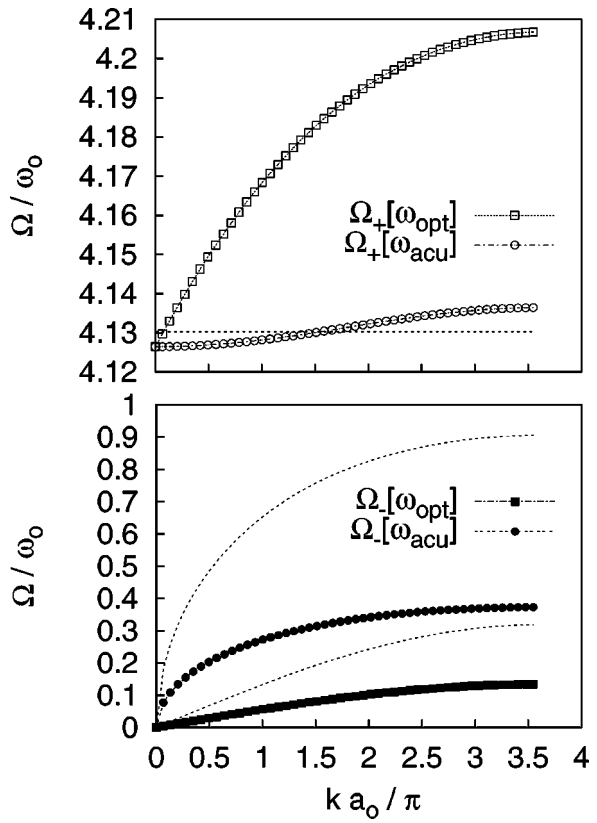

FIG. 8. 2D case. The eigenfrequencies of system along the direction (10) for $\eta=0.9$ and $\alpha=2.12$. $1/r_s=8\times10^{-3}$(a.u.), $T=2.5\times10^{-5}$(a.u.). Density is close to the classical liquid-solid transition. Upper panel: The frequencies of polaronic branch weakly dispersed around the polaronic frequency $\omega_{\mathrm{pol}}\simeq v$ (dashed line). Lower panel: The renormalized Wigner crystal branches (points) and the pure WC branches (dashed lines).

Related to the different 2D and 3D DOS we note the different behavior of the frequencies of the normal modes. Notably, the "optical" branches go to zero as $\sim\sqrt{k}$ at long wavelengths.[52] As in the 3D case, the frequencies of the LPC are split in to four branches (Fig. 8) $\Omega_{\pm}[\omega_{acu}(s,\vec{k})]$ and $\Omega_{\pm}[\omega_{opt}(s,\vec{k})]$ according to the same equation of 3D (see Fig. 8), where the 2D value for ω_W is given in Appendix B [Eq. (B14).

Let us discuss the deviation from the the scaling at strong coupling, which we see from Fig. 2 in the density of the softening of the polaronic frequency ω_{pol}. Actually we observe that a steep fall of the variational parameter $v(r_s)$ occurs as density increases determining the softening of ω_{pol}. Peculiar features of the DOS enter in the variational determination of $v(r_s)$ as can achieved by the following argument. First of all we assume that w is very close to the value ω_{LO} at strong coupling. Then we note that as in the 3D high-polarizability case the renormalized plasma frequency is much less than the phonon frequency, and the discussion which follows Eq. (36) holds for all densities lower than critical density of the softening. In this case the spectrum is composed by the low-energy branches (renormalized WC) and by the polaronic branches weakly dispersed around v (see also Fig. 8). Using this result at low temperatures ($\beta\rightarrow\infty$), the condition for the extrema of $\mathcal{F}_V$ reads

$$1-\frac{1}{v^{3/2}}\sqrt{\frac{\omega_P^2}{\omega\varepsilon_o}}\mathcal{M}_2+g(\alpha,\eta,r_s,v)=0, \tag{51}$$

where the first and second terms are the derivative of $\mathcal{F}_T$ [Eq. (C13)] and g is the derivative of Eqs. (C14), (C15), and (C17). As $v(r_s)\rightarrow0$ for $r_s\simeq r_c$ the second term acquires importance and DOS enters in the second moment $\mathcal{M}_2$. However there are other terms that are divergent as $v\rightarrow0$ coming from the explicit form of the function g.

V. CONCLUSIONS

We have studied the behavior of a low-density electron gas in the presence of a polarizable medium, where polaronic effects may play a relevant role. To determine the transition line, we have used a generalized Lindemann criterion, which reproduces correctly the pure electron gas quantum melting. Because the amplitude of quantum fluctuations depends on the e-ph renormalized plasma frequency, the Lindemann rule has been critically reexamined and adapted to the polaron crystal. This procedure allows one to determine, quantitatively, the phase diagram of the model and to extend the study of the model to the low-polarizability case. We have also studied the 2D case, showing that the dimensional dependence is not crucial to determining the nature of the quantum melting within in our harmonic variational scheme. The scaling predicted for the e-ph coupling constant at zero density does apply as well at nonzero density up to quantum melting. A notable difference instead is in the position of the softening density of the polaronic frequency, which in 3D is much closer to melting than in 2D case. This suggests that the heterointeractions are less effective to destabilize the dipolar crystal in 2D. However other possible mechanisms (lattice effects, structural disorder, or impurities) can cooperate with the localization, together with the interactions between the electrons, and lead to the formation of a pinned Wigner crystal. In this case the melting cannot be predicted by the Lindemann rule, but a similar dipolar instability due to the long-range interaction between the electrons can still drives the melting.

While the weak e-ph coupling regime is similar for both low- and high-polarization cases, the strong coupling scenario is qualitatively different.

In the high-polarizability regime, we have recovered the incipient instability that was found in previous studies near the solid phase[29,30] and also in the liquid phase.[31] In comparison to previous work, we have found that this regime is restricted to very large values of the coupling $\alpha>10$, leaving an interesting intermediate region of coupling in which polarons may exist in the liquid phase. This region can, in principle, be explored with nonperturbative numerical techniques, e.g., path integral Monte Carlo. Work along this direction is currently in progress.

In the low-polarizability regime, a crossover occurs inside the solid phase when the renormalized plasma frequency approaches the phonon frequency. At low density, we still have a LPC, whereas at higher densities the electron-phonon in-

teraction is weakened irrespective of the *bare* electron-phonon coupling. In this case, polaron clouds overlap and the polaron feature of the crystal is lost. The crossover from polaronic ($\omega_P < \omega_{LO}$) to nonpolaronic ($\omega_P > \omega_{LO}$) character has been observed in weakly coupled systems, such as GaAs in the liquid phase, and analyzed in terms of RPA.[22,55] In this system it occurs around $r_s \sim 0.6-0.7$, while for ZnO α is if larger, shifting the crossover to $r_s \sim 7$. Finding a system with low polarizability and a larger e-ph coupling is difficult because it implies very low ω_{LO}: $\alpha \sim (1-\eta)/\omega_{LO}$ [from Eq. (11)]. However in surfaces of InSb, an $\alpha = 4.5$ has been predicted together with $\eta = 0.88$[11] leading to the possible observation of the crossover inside the solid phase.

We also note that our low-polarizability scenario of density crossover inside the solid phase bears some resemblance to that found for ripplonic polaron systems.[58,59] Although the electron-ripplon interaction in these systems is different from the Fröhlich type, resonances in the absorption spectrum observed by Grimes and Adams,[60] their explanation at low density[61] relys on the same qualitative arguments developed in the present work. Recent works on high-density ripplonic polaron systems realized on a helium bubbles predicts also in this case a mixing between plasmon and polaron modes.[62]

Finally, we remark that we have obtained an appreciable stabilization of the crystal phase even for the intermediate regime $\alpha \sim 3$–5 in low-polarizability cases. We conclude that the general result that e-ph interaction effects can stabilize the Wigner crystal phase could motivate experimental studies on two-dimensional electronic devices involving polarizable media. To this aim a layered configuration is advised even with some warnings.[63] In a 2D heterostructure the use of a perpendicular electric field[63] could not only increase the polaron effect but also tune it, as was shown in the case of charged helium surfaces.[64]

ACKNOWLEDGMENTS

The authors acknowledge S. Fratini and P. Quemerais for useful discussions. We also thank J. Lorenzana for useful suggestions. One of us (G.R.) thanks also the kind hospitality of CNRS-LEPES Grenoble, where a part of this work was done. This work was financially supported by MIUR-Cofin 2001 and MIUR-Cofin 2003 matching fund programs.

APPENDIX A: LOW-ENERGY CUTOFF IN 2D

The 2D DOS function can be defined as

$$\rho(\omega) = \sum_{s=1,2} \int_{V_B} d^2k\ \delta(\omega - \omega_{s,k}), \tag{A1}$$

where V_B is the volume of the first Brillouin zone (1 BZ). Let us consider a small fraction ε of the plasma frequency ω_P. At long wavelength ($k=0$), we have the 2D dispersion laws for the acoustical mode as $\omega_1(k) \simeq c_1 k$, while the "optical" $\omega_2(k) \simeq c_2\sqrt{k}$.[46] As a consequence the behavior of the DOS for $\omega \simeq 0$ is

$$\int_0^{2\pi} d\theta \int_0^{k(\varepsilon)} dk\, k\delta(\omega - c_1 k) = \frac{2\pi}{c_1^2}\omega, \tag{A2}$$

$$\int_0^{2\pi} d\theta \int_0^{k(\varepsilon)} dk\, k\delta(\omega - c_2\sqrt{k}) = \frac{4\pi}{c_2^4}\omega^3. \tag{A3}$$

Introducing the scaled frequency x defined as $\omega = \omega_P x$ and the quantum parameter η_q Eq. (23), the thermal electronic fluctuation is expressed as an average on the DOS as

$$\langle u^2 \rangle = \frac{\hbar}{m}\left\langle \frac{\coth(\eta_q x)}{x} \right\rangle_{DOS}, \tag{A4}$$

$$= \frac{\hbar}{m}\int dx\, \rho(\omega_P x)\left[\frac{1}{\eta_q x^2} + \eta_q(\alpha_0 + \alpha_2(\eta_q x)^2 + \ldots) \right]. \tag{A5}$$

Since $\rho(\omega_P x) \sim x$ for $x \to 0$, the average in Eq. (A4) converges for any of x^{2n} with $n \geqslant 0$ in the the expansion Eq. (A5). In the $n=-1$ term we consider the infrared cutoff x_c, giving

$$\left\langle \frac{1}{x^2} \right\rangle_{DOS} \simeq \int_{x_c}^{\varepsilon} dx \frac{(2\pi/c_1^2)\omega_P}{x} + \int_{\varepsilon} dx \frac{\rho(\omega_P x)}{x^2}$$
$$\simeq \frac{2\pi\omega_P}{c_1^2}\ln\left(\frac{\varepsilon}{x_c}\right) + \int_{\varepsilon} dx \frac{\rho(\omega_P x)}{x^2}. \tag{A6}$$

This term diverges logarithmically as $x_c \to 0$. However, $\eta_q \to \infty$ as we approach the quantum region. The electronic fluctuation turns out to be cutoff independent if

$$\left\langle \frac{1}{x^2} \right\rangle \ll \eta_q^2 \langle \alpha_0 + \alpha_2(\eta_q x)^2 + \cdots \rangle. \tag{A7}$$

We have chosen for the cutoff frequency $x_c = \omega_{\min}/\omega_P \simeq 5\times 10^{-5}$ so that the condition Eq. (A7) is fulfilled around $\eta_q(T, r_s) \geqslant 10$, which corresponds to a large region inside to the solid phase. By the relation for acoustical long-wave excitation $\omega_{\min} = c_1 k_{\min}$ and $k_{\min} = 2\pi/(r_s\sqrt{N})$, the number of electrons is $N = 5.24\times 10^6$. Our inverse second moment of DOS is $\mathcal{M}_{-2} = 12.5$ (c.f., Ref. 53, $\mathcal{M}_{-2} = 8.16$ for $N = 1024$).

APPENDIX B: HARMONIC VARIATIONAL APPROXIMATION

We expand in the harmonic approximation the terms $\mathcal{S}_{e-e}$, $\mathcal{S}_{e-J}$, $\mathcal{S}^{\text{dist}}_{e-ph-e}$ [Eqs. (6), (8), and (9)]. Let $\vec{r}_l = \vec{R}_l + \vec{u}_l$, where $\vec{R}_l$ is the lattice point of the crystal and $\vec{u}_l$ is the electronic displacement from $\vec{R}_l$, and set $\Delta\vec{u}_{l,j}(\tau,\sigma) = \vec{u}_j(\sigma) - \vec{u}_l(\tau)$ and $\vec{R}_{j,l} = \vec{R}_j - \vec{R}_l$. The static terms give

$$\mathcal{S}^o_{e-e}(\{\vec{R}_l\}) + \mathcal{S}^o_{e-J}(\{\vec{R}_l\}) + \mathcal{S}^{o,\text{dist}}_{e-ph-e}(\{\vec{R}_l\}) = \frac{\mathcal{S}^o_{\text{WC}}(\{\vec{R}_l\})}{\varepsilon_0} \tag{B1}$$

the e-ph interaction does not change the equilibrium positions of the pure electronic crystal (WC), which corresponds to the minimum of the potential energy.

The sum of the dynamical parts in the harmonic approximation gives

$$\mathcal{S}^H_{e-e} + \mathcal{S}^H_{e-J} + \mathcal{S}^{H,\mathrm{dist}}_{e-ph-e} = \int_0^\beta d\tau \sum_\imath \{V_J[\vec{u}_\imath(\tau)] + V_{e-e}[\vec{u}_\imath(\tau)]\}, \tag{B2}$$

where

$$V_J[\vec{u}_\imath(\tau)] = -\frac{e^2\rho_J}{\varepsilon_0}\int d^D r\left[\frac{1}{|\vec{u}_\imath(\tau)-\vec{r}|}-\frac{1}{r}\right], \tag{B3}$$

$$V_{e-e}[\vec{u}_\imath(\tau)] = \frac{e^2}{2}\int_0^\beta d\sigma F(\tau-\sigma)\sum_{j\neq\imath} U_{j,\imath}(\tau,\sigma), \tag{B4}$$

$$U_{j,\imath}(\tau,\sigma) = \frac{1}{2}\Delta\vec{u}_{\imath,j}(\tau,\sigma)\cdot\overline{\mathcal{I}}(\vec{R}_{j,\imath})\Delta\vec{u}_{\imath,j}(\tau,\sigma), \tag{B5}$$

$$F(\tau-\sigma) = \frac{\delta(\tau-\sigma)}{\varepsilon_\infty} - \frac{\omega_{LO}}{2\overline{\varepsilon}}D_o(\tau-\sigma), \tag{B6}$$

$$[\overline{\mathcal{I}}_{\imath j}]_{\alpha\beta} = \frac{\delta_{\alpha\beta}}{|\vec{R}_{j,\imath}|^3} - 3\frac{[\vec{R}_{j,\imath}]_\alpha[\vec{R}_{j,\imath}]_\beta}{|\vec{R}_{j,\imath}|^5}. \tag{B7}$$

From now we drop on the double σ, τ indexes in $\Delta\vec{u}_{\imath,j}$. To evaluate the integral in Eq. (B3) and the sums on index j in Eq. (B4), we consider a sphere S_R of radius R_s (a disk in 2D) centered on site $\imath$. We first sum on index j and then we perform the limit $R_s\to\infty$. Finally, we sum on index $\imath$ in Eq. (B2).

1. 3D case

By Gauss's law [with the condition $V_J(0)=0$], we have

$$V_J[\vec{u}_\imath(\tau)] = \frac{1}{2}m\frac{\omega_W^2}{\varepsilon_0}|\vec{u}_\imath(\tau)|^2, \tag{B8}$$

where the Wigner frequency is $\omega_W^2=\omega_P^2/3$. Because of V_J is independent of the size of S_R, Eq. (B8) does not change in the limit $R_s\to\infty$.

To evaluate the sum in Eq. (B4) with the condition $R_j < R_s$, we remind that we have two self terms [(i,i) and (j,j)] and two distinct terms [(i,j) and (j,i)] in Eq. (B5). The two self terms give the same contribution, as can be easily checked if we first carry on the limit $R_s\to\infty$ and then the sum on index j and $\imath$. They vanishes because of cubic symmetry of the lattice. When the two distinct terms [(i,j) and (j,i)] of Eq. (B5) are inserted into Eq. (B4) and the limit $R_s\to\infty$ is taken, we obtain the term $V_{e-e}(u_\imath)$ of Eq. (B2)

$$V_{e-e}[\vec{u}_\imath(\tau)] = \frac{e^2}{2}\sum_{j\neq\imath}\int_0^\beta d\sigma F(\tau-\sigma)\vec{u}_j(\sigma)\overline{\mathcal{I}}(\vec{R}_{j,\imath})\vec{u}_\imath(\tau). \tag{B9}$$

Summing on index $\imath$ and integrating on variable τ [Eqs. (B8) and (B9)], we obtain the terms $\mathcal{S}^H_{e-J}$, $\mathcal{S}^H_{e-e}$, $\mathcal{S}^{H,\mathrm{dist}}_{e-ph-e}$ Eqs. (19) and (20).

2. 2D case

In 2D the interaction potential $V_J^R(u)$ of a uniform positively charged disk of radius R_s [Eq. (B3)] is

$$V_J^R(u) = -\frac{e^2\rho_J}{\varepsilon_0}\int_0^{2\pi} d\theta F(\theta), \tag{B10}$$

where

$$F(\theta) = \sqrt{R_s^2+u^2-2R_s u\cos(\theta)} - u - R_s + u\cos(\theta)\ln\frac{R_s - u\cos(\theta)+\sqrt{R_s^2+u^2-2R_s u\cos(\theta)}}{u[1-\cos(\theta)]}.$$

In the limit $R_s\to\infty$

$$\lim_{R\to\infty} V_J^R(\vec{u}_\imath) = \lim_{(u/R)\to 0}\frac{e^2}{\varepsilon_0}\rho_J\frac{\pi}{R_S}u_\imath^2 = 0 \tag{B11}$$

since the total electric field of an infinitely charged disk is perpendicular to the disk.

Then we have to evaluate the sums [Eq. (B5)]. The two distinct terms [(i,j) and (j,i)] give the identical result [Eq. (B9)] of the 3D case, while the self term $(\imath,\imath)$ is written as

$$\frac{1}{2}\vec{u}_\imath\left(\sum_{\substack{\vec{R}_j<R\\ j\neq\imath}}\overline{\mathcal{I}_{\imath j}}\right)\vec{u}_\imath = \vec{u}_\imath\overline{\mathcal{D}}\vec{u}_\imath. \tag{B12}$$

The matrix $\mathcal{D}$ in 2D is defined as sum of the matrices $\overline{\mathcal{I}}(\vec{R}_j)$ [Eq. (B7)] on hexagonal lattice points $\vec{R}_j$. Contrary to the 3D case, the matrix $\mathcal{D}$ is not zero in 2D case. By the lattice symmetry, the off-diagonal elements are zero while the diagonal terms are equal to the local potential, which acts on each electron

$$\frac{e^2}{2}\int_0^\beta d\sigma F(\tau-\sigma)\overline{\mathcal{D}}_{\alpha\alpha}|\vec{u}_\imath(\tau)|^2 = \frac{1}{2}m\frac{\omega_W^2}{\varepsilon_0}|\vec{u}_\imath(\tau)|^2, \tag{B13}$$

where we use as definition 2D Wigner frequency

$$\omega_W^2 = \frac{e^2}{m}\lim_{R\to\infty}\sum_{\substack{j\neq\imath\\ R_{j,\imath}<R}}\frac{1}{2R_{j,\imath}^3} \quad (2\mathrm{D}). \tag{B14}$$

For an hexagonal lattice of nearest-neighbor distance d_{NN}, we have $\Sigma_{j\neq\imath}(1/2R_{j,\imath}^3)=5.517\,09/d_{NN}^3$. Summing on index $\imath$ [Eqs. (B9) and (B13)], we obtain the terms $\mathcal{S}^H_{e-J}$, $\mathcal{S}^H_{e-e}$, $\mathcal{S}^{H,\mathrm{dist}}_{e-ph-e}$ [Eqs. (19) and (20)].

3. Normal modes

The WC normal modes are defined as

$$\vec{u}_\iota = \frac{1}{\sqrt{N}} \sum_{\vec{k},s} \hat{\varepsilon}_{\vec{k},s} q_{\vec{k},s} e^{i\vec{k}\vec{R}_\iota}, \tag{B15}$$

where the vectors $\vec{k}$ belongs to the 1 BZ of the reciprocal lattice, $\hat{\varepsilon}_{\vec{k},s}$ are eigenvectors with eigenvalue $\omega^2_{\vec{k},s}$ of the dynamical matrix $\overline{\mathcal{M}}$, which is defined as

$$\overline{\mathcal{M}}_{\alpha\beta} = \delta_{\alpha\beta}\omega_W^2 + \frac{e^2}{m} \sum_{\vec{R}_\iota \neq 0} \overline{\mathcal{I}}_{\alpha\beta}(\vec{R}_\iota) e^{i\vec{k}\cdot\vec{R}_\iota}. \tag{B16}$$

Inserting the WC normal modes of Eq. (B15) into Eqs. (16) and (18)–(20), we express the harmonic variational action $\mathcal{S}_T$ as

$$\mathcal{S}_T(\{q_{s,\vec{k}}(\tau)\}) = \sum_{s,\vec{k}} \int_0^\beta d\tau L_{s,k}(\tau), \tag{B17}$$

where the Lagrangian is

$$\begin{aligned} L_{s,k} = {} & \frac{1}{2} m |\dot{q}_{\vec{k},s}(\tau)|^2 + \frac{1}{2} m \frac{\omega^2_{\vec{k},s}}{\varepsilon_0} |q_{\vec{k},s}(\tau)|^2 \\ & + \frac{mw(v^2 - w^2)}{8} \int_0^\beta d\sigma D_V(\tau - \sigma) |q_{\vec{k},s}(\tau) - q_{\vec{k},s}(\sigma)|^2 \\ & + \frac{m\omega_{LO}(\omega^2_{\vec{k},s} - \omega_W^2)}{8\overline{\varepsilon}} \int_0^\beta d\sigma D_o(\tau - \sigma) |q_{\vec{k},s}(\tau) - q_{\vec{k},s}(\sigma)|^2. \end{aligned} \tag{B18}$$

APPENDIX C: VARIATIONAL FREE ENERGY $\mathcal{F}_V$

The first term of the variational free energy $\mathcal{F}_V$ [Eq. (21)] is the free energy $\mathcal{F}_T$ associated with the partition function of the trial action $\mathcal{Z}_T$. This is calculated as the functional integral [Eq. (3)], where $\mathcal{S}_{eff}$ [Eq. (4)] is replaced by $\mathcal{S}_T$ [Eq. (17)]. The second term of $\mathcal{F}_V$ is the mean value [Eq. (14)] of the difference between $\mathcal{S}^{\text{self}}_{e-ph-e}$ [Eq. (7)] and $\mathcal{S}_{\text{Feyn}}$ [Eq. (16)].

We start by changing the dynamical variables of integration from $\{\vec{u}_\iota(\tau)\}$ to $\{q_{s,\vec{k}}(\tau)\}$. By reality condition we have $q_{-\vec{k},s} = q^*_{\vec{k},s}$ and $\hat{\varepsilon}_{-\vec{k},s} = -\hat{\varepsilon}_{\vec{k},s}$; we must sum only $\vec{k}$ vectors in the upper half space ($k_z > 0$) of 1 BZ

$$\vec{u}_\iota = \frac{1}{\sqrt{N}} \sum_{s,\vec{k},k_z>0} \hat{\varepsilon}_{\vec{k},s} (q_{\vec{k},s} e^{i\vec{k}\vec{R}_\iota} - q^*_{\vec{k},s} e^{-i\vec{k}\vec{R}_\iota}). \tag{C1}$$

Therefore, the real and imaginary part of $q_{s,\vec{k}}$ for all k with ($k_z > 0$) of the 1 BZ are the actual independent variables and the Jacobian of canonical transformation is $J = 2^{DN}$

$$\mathcal{Z}_T = \int J \prod_{s,\vec{k},k_z>0} \mathcal{D}[q^{\text{Re}}_{s,\vec{k}}(\tau)] \mathcal{D}[q^{\text{Im}}_{s,\vec{k}}(\tau)] e^{-\mathcal{S}_T[\{q_{s,\vec{k}}(\tau)\}]}. \tag{C2}$$

Using the periodicity condition $[q_{s,\vec{k}}(0) = q_{s,\vec{k}}(\beta)]$, we have the following Fourier expansion $[\omega_n = (2\pi/\beta)n]$:

$$q_{s,\vec{k},n} = \frac{1}{\beta} \int_0^\beta d\tau\, q_{s,\vec{k}}(\tau) e^{-i\omega_n \tau}, \tag{C3}$$

$$q_{s,\vec{k}}(\tau) = q_{s,\vec{k},c} + \delta q_{s,\vec{k}}(\tau), \tag{C4}$$

$$q_{s,\vec{k},c} = \frac{1}{\beta} \int_0^\beta d\tau\, q_{s,\vec{k}}(\tau),$$

$$\delta q_{s,\vec{k}}(\tau) = \sum_{\substack{n=-\infty \\ n\neq 0}}^{\infty} q_{s,\vec{k},n} e^{i\omega_n \tau}, \tag{C5}$$

where we have separated the mean value of path on the imaginary time Eq. (C4) (centroid) from the fluctuation around it Eq. (C5). The action $\mathcal{S}_T(\{q_{s,\vec{k}}(\tau)\})$ is quadratic in $\{q_{s,\vec{k},n}\}$, therefore, we can separate Eq. (C2) in two Gaussian integrals

$$\mathcal{Z}_T = \mathcal{Z}_{T,c} \mathcal{Z}_{T,\delta q}, \tag{C6}$$

$$\begin{aligned} \mathcal{Z}_{T,c} &= \int \prod_{s,\vec{k},k_z>0} \frac{dq^{\text{Re}}_{\vec{k},s,c} dq^{\text{Im}}_{\vec{k},s,c}}{\pi\hbar^2/mk_BT} e^{-\mathcal{S}^c_T\{q_{s,\vec{k},c}\}} \\ &= \int \prod_{s,\vec{k},k_z>0} \frac{dq^{\text{Re}}_{\vec{k},s,c} dq^{\text{Im}}_{\vec{k},s,c}}{\pi\hbar^2/mk_BT} e^{-(m|q_{\vec{k},s,c}|^2/k_BT\omega^2_{s,\vec{k}}/\varepsilon_0)} \\ &= \prod_{s,\vec{k}} \frac{k_BT}{\hbar\omega_{s,\vec{k}}/\sqrt{\varepsilon_0}}. \end{aligned} \tag{C7}$$

Hence, after we omit the classic term $\mathcal{Z}_{T,c}$ [Eq. (C7)]

$$\begin{aligned} \mathcal{Z}_{T,\delta q} &= \int \prod_{\substack{n\neq 0 \\ s,\vec{k},k_z>0}} \frac{dq^{\text{Re}}_{\vec{k},s,n} dq^{\text{Im}}_{\vec{k},s,n}}{\pi k_BT/m\omega_n^2} e^{-\delta\mathcal{S}_T\{\delta q_{s,\vec{k}}(\tau)\}} \\ &= \int \prod_{\substack{n\neq 0 \\ s,\vec{k},k_z>0}} \frac{dq^{\text{Re}}_{\vec{k},s,n} dq^{\text{Im}}_{\vec{k},s,n}}{\pi k_BT/m\omega_n^2} e^{-(m/k_BT)(|q_{\vec{k},s,n}|^2/\lambda_{s,\vec{k},n})} \\ &= \prod_{\substack{n\neq 0 \\ s,\vec{k},k_z>0}} \omega_n^2 \lambda_{s,\vec{k},n}, \end{aligned} \tag{C8}$$

where

$$\lambda_{s,\vec{k},0} = \frac{1}{\omega^2_{\vec{k},s}/\varepsilon_0}, \tag{C9}$$

$$\lambda_{s,\vec{k},n} = \sum_{\gamma=1}^{3} \frac{A_\gamma}{\omega_n^2 + \Omega_\gamma^2}, \tag{C10}$$

$$A_1 = \frac{(\Omega_1^2 - \omega_{LO}^2)(\Omega_1^2 - w_T^2)}{(\Omega_1^2 - \Omega_2^2)(\Omega_1^2 - \Omega_3^2)} \quad \text{(cyclic perm. } \gamma = 1,2,3), \tag{C11}$$

the frequencies Ω_γ^2 (γ=1, 2, 3) are the opposite of the roots of cubic

$$\mathcal{P}_3(z) = z^3 + a_2 z^2 + a_1 z + a_0 \tag{C12}$$

$$a_2 = v^2 + \omega_{LO}^2 + \frac{\omega_{\vec{k},s}^2}{\varepsilon_0} + \frac{\omega_{\vec{k},s}^2 - \omega_W^2}{\overline{\varepsilon}}$$

$$a_1 = \omega_{LO}^2 v^2 + \frac{\omega_{\vec{k},s}^2}{\varepsilon_0}(\omega_{LO}^2 + w^2) + w^2 \frac{\omega_{\vec{k},s}^2 - \omega_W^2}{\overline{\varepsilon}}$$

$$a_0 = \frac{\omega_{LO}^2 w^2 \omega_{\vec{k},s}^2}{\varepsilon_0}.$$

The Gaussian integrals Eq. (C8) are convergent if $\lambda_{s,\vec{k},n}$ are positive numbers $\forall(s,\vec{k},n)$. This condition is fulfilled if Ω_γ^2 are *all* positive. The numerical minimization of the variational free energy has been made enforcing this constraint. Performing the infinite product in Eq. (C8) we have

$$\mathcal{Z}_{T,\delta q} = \left[\frac{\sinh(\hbar\omega_{LO}/2k_BT)}{\hbar\omega_{LO}/2k_BT}\right]^{DN}\left[\frac{\sinh(\hbar w/2k_BT)}{\hbar w/2k_BT}\right]^{DN} \cdot \prod_{s,\vec{k},\gamma} \frac{\hbar\Omega_{\gamma,s,\vec{k}}/2k_BT}{\sinh(\hbar\Omega_{\gamma,s\vec{k}}/2k_BT)}$$

and finally we substitute the sum on $(\vec{k}_i, s)$ with the integral on the WC DOS $\rho(\omega)$ in the free energy $\mathcal{F}_T$

$$\frac{\mathcal{F}_T}{DN} = -k_BT\ln\left[\sinh\left(\frac{\hbar\omega_{LO}}{2k_BT}\right)\sinh\left(\frac{\hbar w}{2k_BT}\right)\right] + k_BT\int d\omega\rho(\omega)\sum_{\gamma=1}^{3}\ln\left[\sinh\left(\frac{\hbar\Omega_\gamma(\omega)}{2k_BT}\right)\right]. \tag{C13}$$

To calculate the mean value of $\mathcal{S}_{e\text{-}ph\text{-}e}^{\text{self}}$ [Eq. (7)] in 3D we use the following identity[57]

$$\int\int_0^\beta d\tau d\sigma D_o(\tau-\sigma)\int\frac{d^3q}{(2\pi)^3}\frac{4\pi}{q^2}\langle e^{i\vec{q}\cdot[\vec{u}_l(\tau)-\vec{u}_l(\sigma)]}\rangle_T = -2\beta\int_0^{\beta/2} d\tau\frac{D_o(\tau)}{\sqrt{(\pi/2)d_{3D}(\tau)}}, \tag{C14}$$

while in $2D(q^2=q_\perp^2+q_z^2)$

$$\int\int_0^\beta d\tau d\sigma D_o(\tau-\sigma)\int\frac{d^2q_\perp}{(2\pi)^2}\frac{2\pi}{q_\perp}e^{-(1/2)d_{2D}(\tau-\sigma)q_\perp^2} = -2\beta\left(\frac{\pi}{2}\right)\int_0^{\beta/2} d\tau\frac{D_o(\tau)}{\sqrt{(\pi/2)d_{2D}(\tau)}}, \tag{C15}$$

where $d_D(\tau)$ is the imaginary time diffusion in the LPC defined as (3D or 2D)

$$d_D(\tau) = \frac{\langle|\vec{u}(\tau)-\vec{u}(0)|^2\rangle_T}{D}. \tag{C16}$$

The mean value of $\mathcal{S}_{\text{Feyn}}$ [Eq. (16)] is

$$\langle\mathcal{S}_{\text{Feyn}}\rangle_T/N = -D\frac{mw(v^2-w^2)}{8}\int\int_0^\beta d\tau d\sigma D_T(\tau-\sigma)d_D(\tau-\sigma). \tag{C17}$$

To obtain Eqs. (C14), (C15), and (C17) we have used

$$\langle e^{i\vec{q}\cdot[\vec{u}_l(\tau)-\vec{u}_l(\sigma)]}\rangle_T = e^{-(1/2)d_D(\tau-\sigma)q^2}. \tag{C18}$$

We will demonstrate Eq. (C18) in the next section.

1. Calculation of $\langle\exp\{i\vec{q}\cdot[\vec{u}_l(\tau)-\vec{u}_l(\sigma)]\}\rangle_T$

From Eqs. (B15) and (C5) we have

$$i\vec{q}\cdot[\vec{u}_l(\tau)-\vec{u}_l(\sigma)] = \sum_{\substack{s,k_z>0\\ n\neq 0}}[q_{\vec{k},s,n}J_{s,k,n}^*(\tau-\sigma,\vec{q}) + \text{c.c.}], \tag{C19}$$

$$J_{s,k,n}^*(\tau-\sigma,\vec{q}) = \frac{i}{\sqrt{N}}\vec{q}\cdot\hat{\varepsilon}_{\vec{k},s}(e^{i\omega_n\tau}-e^{i\omega_n\sigma})e^{i\vec{k}\vec{R}_l}, \tag{C20}$$

then we have

$$\langle\exp(i\vec{q}\cdot[\vec{u}_l(\tau)-\vec{u}_l(\sigma)])\rangle_T = \frac{1}{\mathcal{Z}_{T,\delta q}}\int\prod_{\substack{n\neq 0\\ s,\vec{k},k_z>0}}\frac{dq_{\vec{k},s,n}^{\text{Re}}dq_{\vec{k},s,n}^{\text{Im}}}{\pi k_BT/m\omega_n^2}e^{-(m/k_BT)(|q_{\vec{k},s,n}|^2/\lambda_{s,\vec{k},n})+q_{\vec{k},s,n}J_{\vec{k},s,n}^*+\text{c.c.}} = \prod_{\substack{s,k_z>0\\ n\neq 0}}e^{-(k_BT/m)\lambda_{s,\vec{k},n}|J_{\vec{k},s,n}|^2}$$

$$= e^{-(1/2)(1/N)\sum_{s,k}|\hat{q}\cdot\hat{\varepsilon}_{\vec{k},s}|^2 d_{\omega_{s,k}}(\tau-\sigma)q^2} = e^{-(1/2)(1/ND)\sum_{s,k}d_{\omega_{s,k}}(\tau-\sigma)q^2} = e^{-(1/2)d_D(\tau-\sigma)q^2}, \tag{C21}$$

where the component of frequency $\omega_{s,k}$ of the imaginary time diffusion $d_D(\tau)$ is $[A_\gamma = A_\gamma(\omega_{s,k}), \Omega_\gamma = \Omega_\gamma(\omega_{s,k})]$

$$d_D(\tau) = \frac{1}{ND}\sum_{s,k} d_{\omega_{s,k}}(\tau)$$
$$= \frac{1}{ND}\sum_{s,k}\frac{\hbar}{m}\sum_\gamma \frac{A_\gamma}{\Omega_\gamma^2}\frac{\cosh(\beta\Omega_\gamma/2) - \cosh(\Omega_\gamma[\beta/2 - \tau])}{\sinh(\beta\Omega_\gamma)}. \tag{C22}$$

APPENDIX D: MEAN ELECTRONIC FLUCTUATION

The relation between the mean electronic fluctuation and the imaginary time diffusion $d_D(\tau)$ Eq. (C16) is

$$d_D(\tau) = \frac{2}{D}[\langle|\vec{u}(0)|^2\rangle - \langle\vec{u}(\tau)\cdot\vec{u}(0)\rangle] \tag{D1}$$

comparing Eq. (D1) and Eq. (C22) for $d_D(\tau)$ and inserting the DOS function, we have

$$\sigma_T^2 = \frac{\langle|\vec{u}|^2\rangle}{D} = \int d\omega\rho(\omega)\sum_{\gamma=1}^{3}\frac{\hbar A_\gamma(\omega)}{2m\Omega_\gamma^2(\omega)}\coth\left(\frac{\beta\Omega_\gamma(\omega)}{2}\right). \tag{D2}$$

If we fix $w=\omega_o$, we have $\Omega_3=\omega_o$ for one solution of the cubic polynomial Eq. (C12) and by Eq. (C11) we have also $A_3=0$. The other two terms give

$$\langle u^2\rangle_+ = \int d\omega\rho(\omega)\frac{\Omega_1^2-\omega_{LO}^2}{\Omega_1^2-\Omega_2^2}\frac{\hbar D}{2m\Omega_1}\coth\left(\frac{\hbar\Omega_1}{2k_BT}\right), \tag{D3}$$

$$\langle u^2\rangle_- = \int d\omega\rho(\omega)\frac{\Omega_2^2-\omega_{LO}^2}{\Omega_2^2-\Omega_1^2}\frac{\hbar D}{2m\Omega_2}\coth\left(\frac{\hbar\Omega_2}{2k_BT}\right). \tag{D4}$$

Note that if we take a single Wigner frequency being representative of the electronic spectrum $[\rho(\omega)=\delta(\omega-\omega_W)]$ we recover the results of Ref. 29.

APPENDIX E: POLARON RADIUS

We now calculate the density-density correlation function of the Eq. (32) for the variational harmonic action $\mathcal{S}_T$. We assume that the equilibrium position of the reference electron $\imath=1$ is the origin. With the same method to obtain Eqs. (C21), we performed the following Gaussian integrals for the density distribution $\rho_1(\vec{r})$

$$\langle\hat{\rho}_1(\vec{r})\rangle_T = \int\frac{d^Dq}{(2\pi)^D}e^{i\vec{q}\vec{r}_e}\langle e^{i\vec{u}_1\vec{q}}\rangle_T = \frac{e^{-r^2/2\sigma_T^2}}{[2\pi\sigma_T^2]^{D/2}} \tag{E1}$$

and

$$\langle e^{-i\vec{q}\vec{u}_1}e^{i\vec{q}'(\vec{u}_1(\tau)-\vec{u}_1)}\rangle_T = e^{-(\sigma_T^2/2)q^2}e^{-(d(\tau)/2)\vec{q}'\cdot[\vec{q}'+\vec{q}]}. \tag{E2}$$

Inserting Eq. (E2) into Eq. (32), we have the density-density correlation function in the imaginary-time for the $\imath=1$ electron

$$\langle\rho_1(\vec{r})\rho_1(\vec{r}',\tau)\rangle_T = \langle\hat{\rho}_1(\vec{r})\rangle_T\frac{e^{-[|\vec{r}-\vec{r}'+(d(\tau)/2\sigma^2)\vec{r}|^2/2\ell^2(\tau)]}}{[2\pi\ell^2(\tau)]^{D/2}}, \tag{E3}$$

where

$$\ell^2(\tau) = d_D(\tau)\left[1-\frac{d_D(\tau)}{4\sigma_T^2}\right]. \tag{E4}$$

We note that the function of Eq. (E3) does not depend only on the relative distance $\vec{r}'-\vec{r}$ but also on the distance of electron from its localization position in the crystal. Then Eq. (32) becomes

$$C_{1,T}^{\text{self}} = \frac{1}{\varepsilon}\int_0^\beta d\tau\frac{\omega_{LO}}{2}D_o(\tau)\frac{\langle\rho_1(\vec{r})\rho_1(\vec{r}',\tau)\rangle_T}{\langle\rho_1(\vec{r})\rangle_T}. \tag{E5}$$

We assume $\vec{r}=0$ (electron in its lattice point) and then obtain the variational radial-induced charge density

$$g_T(r) = \frac{\pi\omega_{LO}}{2\varepsilon}(2r)^{D-1}\int_0^\beta d\tau D_o(\tau)\frac{e^{-r^2/2\ell^2(\tau)}}{[2\pi\ell^2(\tau)]^{3/2}}. \tag{E6}$$

By Eq. (34) we obtain the variational polaron radius

$$R_{p,T} = \left[\mathrm{D}\frac{\omega_{LO}}{2}\int_0^\beta d\tau D_o(\tau)\ell^2(\tau)\right]^{1/2}. \tag{E7}$$

1. High density limit

The characteristic length $\ell^2(\tau)$ defined in Eq. (E4) is expressed in terms of τ-dependent positional fluctuations $d_D(\tau)$ [Eq. (C16)], which is an integral of a function $d_{\omega_{s,k}}(\tau)$ weighted by the DOS $\rho(\omega)$ of the Wigner lattice [Eq. (C22)]. To have an estimate of this integral we replace the integration by inserting an average frequency in the function $d_{\omega_{s,k}}$. We choose $\omega_P/\sqrt{\varepsilon_\infty}$ because it is the typical frequency of the electronic fluctuation in the crystal for the high-density regime [Eq. (47)]. Moreover, we consider the low-temperature limit ($k_BT \ll \hbar\omega_P/\sqrt{\varepsilon_\infty}$). Then from Eq. (E4) we get the following estimate for $\ell^2(\tau)$:

$$\ell^2(\tau) \simeq \frac{\hbar}{m\omega_P/\sqrt{\varepsilon_\infty}}(1-e^{-2(\omega_P/\sqrt{\varepsilon_\infty})\tau}). \tag{E8}$$

The characteristic time scale of electronic diffusion in imaginary time is $\tau_{el}=(\omega_P/\sqrt{\varepsilon_\infty})^{-1}$. The rising time is $\tau_{el}=1/(2\omega_P/\sqrt{\varepsilon_\infty})$. Therefore, we have approximately

$$\ell^2(\tau) \simeq \frac{\hbar}{m}\tau \quad (\tau \ll \tau_{el}),$$

$$\ell^2(\tau) \simeq \frac{\hbar}{2m\dfrac{\omega_P}{\sqrt{\varepsilon_\infty}}} \quad (\tau \gg \tau_{el}).$$

Now in the variational polaron radius $R_{p,T}$ of Eq. (E7) another time scale appears $\tau_{ph}=\omega_{LO}^{-1}$, but at high density $\tau_{ph} \gg \tau_{el}$. Now we can separate the lowest time scale τ_{el} contri-

bution in the imaginary time integral so that we can approximate the integral in Eq. (E7) as

$$\int_0^{\tau_{el}} d\tau D_o(\tau)\frac{e^{-[r^2/2\ell^2(\tau)]}}{[2\pi\ell^2(\tau)]^{3/2}} \simeq D_o(0)\int_0^{\tau_{el}} d\tau \frac{e^{-\left(r^2/2\frac{\hbar}{m}\tau\right)}}{[2\pi\ell^2(\tau)]^{3/2}} = \frac{m}{2\pi\hbar}\frac{1}{r}\left(1-\mathrm{erf}\sqrt{\frac{r^2}{\langle u^2\rangle}}\right)$$

$$\int_{\tau_{el}}^{\beta} d\tau D_o(\tau)\frac{e^{-[r^2/2\ell^2(\tau)]}}{[2\pi\ell^2(\tau)]^{3/2}} \simeq \frac{e^{-\left(\frac{r^2/\hbar}{m\omega_P/\sqrt{\varepsilon_\infty}}\right)}}{(2\pi\langle u^2\rangle)^{3/2}}\int_{\tau_{el}}^{\beta} d\tau D_o(\tau) \simeq \frac{e^{-r^2/2\langle u^2\rangle}}{(2\pi\langle u^2\rangle)^{3/2}}.$$

Collecting these results we get Eq. (48).

[1] E. Wigner, Phys. Rev. **46**, 1002 (1934).
[2] Jongsoo Yoon, C. C. Li, D. Shahar, D. C. Tsui, and M. Shayegan Phys. Rev. Lett. **82**, 1744 (1998).
[3] M. D. Jones and D. M. Ceperley, Phys. Rev. Lett. **76**, 4572 (1996).
[4] M. Imada and M. Takahashi, J. Phys. Soc. Jpn. **53**, 3770 (1984); B. Bernu, L. Cândido, and D. M. Ceperley, Phys. Rev. Lett. **86**, 870 (2001).
[5] S. T. Chui and B. Tanatar, Phys. Rev. Lett. **74**, 458 (1995).
[6] *Polarons and Excitons*, edited by C. G. Kuper and G. D. Whitfield (Oliver and Boyd, Edinburgh, 1962).
[7] *Polarons in Ionic Crystals and Polar Semiconductor*, edited by J. Devreese (North Holland, Amsterdam, 1972).
[8] A. Mooradian and G. B. Wright, Phys. Rev. Lett. **16**, 999 (1966).
[9] B. B. Varga, Phys. Rev. **137**, 1896 (1965).
[10] G. Irmer, M. Wenzel, and J. Monecke, Phys. Rev. B **56**, 9524 (1997), and references therein.
[11] Hong Sun and Shi-Wei Gu, Phys. Rev. B **44**, 1163 (1991).
[12] P. Zhang, W. Xiao, and J.-L. Xiao, Physica B **245**, 354 (1998).
[13] N. Kirova and M. N. Bussac, Phys. Rev. B **68**, 235312 (2003); N. Kirova and M. N. Bussac, J. Phys. IV **12**, 99 (2002).
[14] Y. H. Kim, C. M. Foster, A. J. Heeger, S. Cox, and G. Stucky, Phys. Rev. B **38**, 6478 (1988).
[15] C. Taliani, R. Zambone, G. Raum, F. C. Matacotta, and K. I. Pokhadnya, Solid State Commun. **66**, 487 (1988).
[16] S. Lupi, P. Calvani, M. Capizzi, P. Maselli, W. Sadowski, and E. Walker, Phys. Rev. B **45**, 12 470 (1992); P. Calvani, M. Capizzi, S. Lupi, P. Maselli, A. Paolone, and P. Roy, *ibid.* **53**, 2756 (1996).
[17] A. Lanzara, P. V. Bogdanov, X. J. Zhou, S. A. Kellar, D. L. Feng, E. D. Lu, T. Yoshida, H. Eisaki, A. Fujimori, K. Kishio, J.-I. Shimoyama, T. Noda, S. Uchida, Z. Hussain, and Z. X. Shen, Nature (London) **412**, 510 (2001).
[18] S. Fratini and P. Quémerais, Mod. Phys. Lett. B **12**, 1003 (1998).
[19] M. A. Kastner, R. J. Birgeneau, G. Shirane, and Y. Endoh, Rev. Mod. Phys. **70**, 897 (1998).
[20] A. Lucarelli, S. Lupi, M. Ortolani, P. Calvani, P. Maselli, M. Capizzi, P. Giura, H. Eisaki, N. Kikugawa, T. Fujita, M. Fujita, and K. Yamada, Phys. Rev. Lett. **90**, 037002 (2003).
[21] A. V. Puchkov, T. Timusk, M. A. Karlow, S. L. Cooper, P. D. Han, and D. A. Payne, Phys. Rev. B **54**, 6686 (1996).
[22] G. D. Mahan, *Many-Particle Physics* (Plenum, New York, 1981), Chap. 6; G. D. Mahan, in *Polarons in Ionic Crystals and Polar Semiconductors* (Ref. 7), p. 553.
[23] L. F. Lemmens, J. T. Devreese, and F. Brosens, Phys. Status Solidi B **82**, 439 (1977).
[24] G. Iadonisi, G. Capone, V. Cataudella, and G. De Filippis, Phys. Rev. B **53**, 13 497 (1996).
[25] I. Bozovic, Phys. Rev. B **48**, 876 (1993).
[26] G. De Filippis, V. Cataudella, and G. Iadonisi, Eur. Phys. J. B **8**, 339 (1999).
[27] T. D. Lee, F. Low, and D. Pines, Phys. Rev. **90**, 297 (1953).
[28] P. Quémerais, Mod. Phys. Lett. B **9**, 1665 (1995).
[29] S. Fratini and P. Quémerais, Eur. Phys. J. B **14**, 99 (2000).
[30] S. Fratini and P. Quémerais, Eur. Phys. J. B **29**, 41 (2002).
[31] J. Lorenzana, Europhys. Lett. **53**, 532 (2001).
[32] *Polarons and Excitons* (Ref. 6), pp. 29–80.
[33] W. J. Carr, Phys. Rev. **122**, 1437 (1961); See also Sec. II.
[34] R. P. Feynman and A. R. Hibbs, *Quantum Mechanics and Path Integrals* (McGraw-Hill, New York, 1965).
[35] G. Verbist, M. A. Smondyrev, F. M. Peeters, and J. T. Devreese, Phys. Rev. B **45**, 5262 (1992).
[36] The pure electron gas limit of action Eq. (4) can be reached when $\alpha=0$ and α_e is finite, which *implies* $\eta=1$. On the other hand, for a given η, $\alpha_e\to 0$ as $\alpha\to 0$. It should be noted, however, that the limit of zero e-ph interaction is somehow unphysical in the presence of a given inverse polarizability parameter of the system, as can be seen by the calculation of Appendix B, when $\varepsilon_0\neq\varepsilon_\infty$, the interaction with the polarizable medium is *necessary* to stabilize the crystal phase (static term).
[37] R. P. Feynman, Phys. Rev. **97**, 660 (1955).
[38] T. D. Schultz, Phys. Rev. **116**, 526 (1969).
[39] R. Mochkovitch and J. P. Hansen, Phys. Lett. **73**, 35 (1979).
[40] H. Nagara, Y. Nagata, and T. Nakamura, Phys. Rev. A **36**, 1859 (1987); See also Ref. 31.
[41] D. Ceperley (private communication); See also Ref. 4.
[42] In this sense the stabilization of the solid phase due to Fermi statistics is here considered not explicitly, since we consider distinguishable particles, but phenomenologically via the fitted parameter $\gamma(\eta_q)$.
[43] Note, however, that this discussion does not involve the left-hand side of Eq. (22) in which ω_P appears as a result of harmonic approximation.
[44] S. Ciuchi, J. Lorenzana, and C. Pierleoni, Phys. Rev. B **62**, 4426 (2000).
[45] N. D. Mermin, Phys. Rev. **176**, 250 (1968).
[46] L. Bonsall and A. A. Maradudin, Phys. Rev. B **15**, 1959 (1977).
[47] R. A. Coldwell-Horsfall and A. A. Maradudin, J. Math. Phys. **1**, 395 (1960).
[48] R. E. Peierls, Helv. Phys. Acta **7** (suppl. 2), 81 (1936); See also, *Quantum Theory of Solids* (Oxford University Press, London, 1955), Part 3.3.
[49] L. D. Landau and E. M. Lifshitz, *Statistical Physics* (Pergamon Press, New York, 1968).

[50] M. Baus, J. Stat. Phys. **22**, 111 (1980).
[51] A. Alastuey and B. Jancovici, J. Stat. Phys. **24**, 443 (1981).
[52] R. S. Crandall, Phys. Rev. A **8**, 2136 (1973).
[53] R. C. Gann, S. Chakravarty, and G. V. Chester, Phys. Rev. B **20**, 326 (1979).
[54] W. B. da Costa and N. Studart, Phys. Rev. B **47**, 6356 (1993).
[55] Wu Xiaoguang, F. M. Peeters, and J. T. Devreese, Phys. Rev. B **32**, 6982 (1985).
[56] F. M. Peeters and J. T. Devreese, Phys. Rev. B **36**, 4442 (1987).
[57] Note that $\ell^2(\tau)$ and $d(\tau)$ are symmetric functions with respect to time $\beta/2$ in the interval $0<\tau<\beta$ as $D_o(\tau)$.
[58] E. Y. Andrei, *Two-Dimensional Electron Systems on Helium and Other Cryogenic Substrates* (Kluwer, Dordrecht, 1997), pp. 245–279 and references therein.
[59] E. Y. Andrei, Phys. Rev. Lett. **52**, 1449 (1984).
[60] C. C. Grimes and G. Adams, Phys. Rev. Lett. **42**, 795 (1979).
[61] D. S. Fisher, B. I. Halperin, and P. M. Platzman, Phys. Rev. Lett. **42**, 798 (1979).
[62] S. N. Klimin, V. M. Fomin, J. Tempere, I. F. Silvera, and J. T. Devreese, Solid State Commun. **126**, 409 (2003); J. Tempere, S. N. Klimin, I. F. Silvera, and J. T. Devreese, Eur. Phys. J. B **32**, 329 (2003).
[63] V. M. Fomin and M. A. Smondyrev, Phys. Rev. B **49**, 12 748 (1994); N. Mori and T. Ando, *ibid.* **40**, 6175 (1989).
[64] S. A. Jackson and P. M. Platzman, Phys. Rev. B **24**, 499 (1981); **25**, 4886 (1982); M. H. Degani and O. Hipolito, *ibid.* **32**, 3300 (1985).